On Simulations of Corticospinal Projections

Master of Science
School of Informatics
University of Sussex
2007

Abstract

The motoneurones that control synergistic muscles have been demonstrated to share a common presynaptic drive [12] [23]. A recent frequency study of Electromyogram (EMG) signals, recorded from short and long thumb abductor muscles, showed significant coherence in the common drive around 20Hz, which can be mapped to cortical oscillations at 20 Hz frequencies [18]. This frequency study provided compelling data showing that EMG-EMG coherence undergoes developmental changes between the ages of 4 until adulthood. This very novel finding is currently unexplained. The differences in coherence are most marked between 7-9 year olds and 12-14 year olds, suggesting that changes occurring during puberty have a notable effect on the structuring of the common drive.

The aim of this project was to develop a simulation of the corticospinal descending and ascending pathways that enabled exploration of the issues surrounding this developmental pattern. Because the changes in common drive occurring during puberty, the simulation provides a rich platform to explore many of the mechanisms that may be responsible for the changes in EMG-EMG coherence including pruning, myelination and the changes in cortical activity,

The project presents a highly parameterised model of corticospinal projections, which includes biological plausible neurone models, synaptic connections and muscles, as well as sources of afferent feedback ignored in previous studies [3] [38] [43] [56]. The model produces a rich set of recordings that support exploration and direct comparison with experimental data.

Acknowledgements

I would like to express my thanks to everyone in the Department of Informatics and my fellow students who made the Evolutionary and Adaptive Systems course so fulfilling. I am indebted to Dr Luc Berthouze for all his support, words of encouragement and good humour as my thesis supervisor.

I am extremely grateful to both Dr Simon Farmer for his expertise at guiding the early stages of this research as well as providing such a stimulating initial paper. I would also thank both Dr Randall Power and Dr Andrew Fuglevand for their kind help when I discovered issues recreating their models.

Lastly and most importantly, I wish to express my heartfelt thanks to my wife Beth for her love, support and dedication during this course. I couldn't have done it without her and to her I dedicate this thesis.

Declaration

I declare that this thesis was composed by myself, that the work contained herein is my own except where explicitly stated otherwise in the text, and that this work has not been submitted for any other degree or professional qualification except as specified.

()

Table of Contents

List of Figures

List of Tables

Chapter 1

Introduction

The mechanistic and biophysical properties of the neural circuits active in controlling movement in human and animal motor control systems have attracted considerable study. Movement arises from the temporal and spatial patterns of muscular contractions controlled by the actions of the spinal cord and brain. Lower motoneurones in the spinal cord innervate muscles in response to signals from local interneurones and from descending pathways from upper motoneurones. The upper motoneurones are primarily innervated by signals from many parts of the brain including the basal ganglia, which primes the motoneurones for movement and helps suppress unwanted movement, and the cerebellum, which helps detect movement error through connections with the somatosenory brain areas [50].

Nevertheless, the actual form of motor commands is not so well understood. Motor commands arise from the complex interactions of many parts of the cortex, requiring the creation of temporary functional assemblies of neurones to achieve a designated task. There is still considerable debate about how information is encoded in the firing patterns of individual and populations of neurones and how these functional assemblies of neurones can be constructed to achieve a given task.

A neurone can transmit information by modifying its firing rate in response to the input stimulus, rate coding, as well as in the timing of its responses with other neurones, temporal coding. If a group of neurones is tuned to similar stimulus, they may all begin firing rhythmically and if that stimulus is organised in a certain way this rhythmic firing may become synchronous. Rhythmic activity in the brain can fall into a number of ranges: Delta ($<$4Hz), Theta (4-7Hz), Alpha (8-13Hz), Beta ($\approx$ 13-24Hz) and Gamma ($>$24Hz - 40Hz) [50] which represent levels of concurrent neural activity.

To achieve smooth movement and muscle control, antagonistic and co-contracting muscles must form functional synergies so that their movements are coordinated. Antagonistic pairs of muscles require that while one muscle contracts, the other relaxes. In co-contracting pairs, the muscles' contractions must be coordinated to achieve the desired overall force or limb position.

One mechanism through which muscle coordination is achieved is through the production of a common drive to the motor-units innervating the muscle pair [12] [14] [18] [29]. Datta et al. reported that '... descending pathways of cortical origin, including branched stem corticospinal axons are important in the generation of short-term synchronisation' [14]. A study by Conway et al. concluded by stating it showed '... direct evidence that cortical activity contributes to the 16-32Hz modulation of motor unit discharges.' [12]. The common drive can be formed through branch shared inputs to the motor-units or through synchronised activity in separate inputs to the motor-units [23] [34].

Frequency analysis of this common drive has shown high levels of coherence ranged across 1-45Hz between cortical activity and motor-unit activity. By comparing Magnetoencephalogram (MEG)- Electormyogram (EMG) and Electroencephalogram (EEG)-EMG, researchers have shown that $\approx$ 20Hz oscillations (Beta range) originate from activity in the corticospinal pathways. The cortical signal recorded from the primary motor cortex has been demonstrated to interact with the muscle signal at $\approx$ 20Hz [12] [27] [18]. However it has been reported in [12] [14] that the oscillatory components of common drive are only present during steady grip part of contractions and are abolished by movement.

In a recent study, Farmer et al. [18] showed that the common drive to synergistic motorneurone pools undergoes highly interesting developmental changes. The study measured surface EMG-EMG coherence for the co-contracting short and long thumb abductor muscles during a isometric grip task. An isometric contraction is one in which the muscle is activated and held at a constant length and there is no movement of the muscle. Farmer's study investigated age-related changes to the common drive and demonstrated that coherence in the recorded EMGs increased strongly in the 4-40Hz range during puberty and was centred around $\approx$20Hz. This developmental change in drive shows that synergistic muscles form closer relationships during puberty and reflected by a significant change in the drive to motor-units which settles on an oscillatory drive at a seemingly fixed frequency.

This novel result is unexplained and raises two important research questions: firstly, under what developmental conditions does such coherence arise? and secondly, what is the functional significance of such oscillations?

The hypothesis of this thesis is that computational neuroscience models of the corticospinal projection can be built that will enable the exploration of the many complex issues surrounding maturation of motor control. Particular design goals will be drawn from these two research questions.

The emergence of oscillations

When considering how oscillations may emerge, it has been shown that disjoint neural groups engaged in the same task will oscillate synchronously [50]. However, the mechanisms under-

pinning this synchronicity are unknown. There are several potential sources for the explanation of synchronised oscillations over long distances. Networks can be driven by common oscillatory input with shared axons conveying the oscillatory components, such as a driving input from a pacemaker neurone. Alternatively, such oscillations are an emergent property of the active network either through its own activity or through multiple inputs combining frequencies and their harmonics.

Studies have shown that oscillatory activity can emerge from a self organised sheet of neurones responding to aperiodic input [45], where feedback forms an important part of shaping the emergent behaviour of the system. Pauluis et al. [45] demonstrated clearly how the properties of the network control the oscillatory frequency that emerged. In this work, the properties of the inhibitory neurones (membrane, synaptic time constants and distribution of delays) and their connections dominated the behaviour of a simulated neural sheet. With only weak inhibition, oscillatory components of the network quickly decayed. The frequency of oscillations could be tuned by changing both the inhibitory conduction delays and in the time course of the inhibitory post-synaptic potentials they invoked. In addition the emergent frequency was also somewhat controlled by input intensity and its distribution, which provided a mechanism for selectively exciting or inhibiting a target network [45].

For voluntary motor control, it is suggest strongly by Gibbs et al. [23] and Riddle & Baker [52] that feedback from afferent sources may play an important part in structuring muscle coherence.

Developmental Issues

Gibbs et al. [23] concluded by stating that the increases in motor-unit synchronicity cannot 'simply be equated with the maturation of corticospinal tract fibres'. Therefore there must be other changes to the organisation of this motor pathway. The brain undergoes massive changes during its developmental process and many cortical areas involved in movement do not reach maturation until adolescence or later [46].

During the design of the simulation three developmental changes were selected as key tasks for the neural simulator to model: changes in EEG frequencies that underlie neural activity, synaptic pruning and changes in conduction velocities.

EEG in humans starts with slow rhythmic activity, which is followed by age-dependent increase in the frequency of background rhythmic activity [10]. Beta frequencies in particular increase between ages of 8 to 12 years and may have a relationship with common drive changes.

During puberty the brain also undergoes large-scale changes reported widely as grey-matter (GM) loss [46]; such matter is formed by unmyelinated axons, glial cells and neural bodies. This GM loss could results in reductions in the connectivity and population of neural tissue involved in the ascending and descending pathways for motor control. Such pruning could

have a both a substantive impact on the structure of the common drive, as well as the functional assemblies created.

Related to the issue of pruning is the increased myelination shown during development. Paus [46] theorised that loss of GM may not be entirely due to synaptic pruning, but instead due to its conversion to white matter through increased myelination. Gogtay et al. [24] state that GM loss may be in part be masked through axonal myelination through the first four decades. This increased myelination may be balanced by the growth of the body during puberty, although as corticospinal tract maturation occurs early [23] it suggests it may also be related to increases in neural activity.

Simulation

To model issues raised in the previous sections, it is inferred that any model of the corticospinal projection must be as biologically plausible as possible, contain sources of feedback, methods to alter the arrangements of common drive to muscles and also to provide signals that support comparison with experimental work [23] [18].

There have been numerous prior studies that have examined sections of the corticospinal projection but no models containing feedback, effectors and EMG generation were discovered during the review period. Baker et al. described a model involving elements of the cortex and spinal cord but with no effector muscle or feedback [5]. Fuglevand et al. [20] and Yao et al. [56] used models of motoneurones and effectors to look at issues of motor-unit synchrony and provide plausible EMG signals. Naussbauer et al. [43] discussed a complex model of the motoneurone pool and matched it with experimental data for the first dorsal interosseous muscle, but modelled neither feedback nor EMG signals. Only one study was uncovered that considered afferent feedback an essential part of the motor-control loop [38], but this signal was used only as an error signal to modulate pre-structured common drive when investigating motor-unit discharge patterns.

The aim of this thesis is to provide a simulation of the entire corticospinal projection that encompasses the principle components of this system including muscle models and afferent feedback. Such a simulation will provide a real investigative tool that can be used to explore the developmental changes in motor-unit common drive.

1.1 Organisation of this thesis

Chapter 2 discusses the principle biological structures involved in the execution of motor commands. Chapter 3 provides a description of the simulator developed to investigate the emergence of coherence in co-contracting muscles, following the basic developmental ideas outline in this chapter. In Chapter 4 simulation results are discussed along. Finally, Chapter 5 discusses

the outcome of the project and current limitations in the model.

Appendix A contains exploratory information regarding the major components of the neural simulation. Appendix B contains Matlab models of individual components and Appendix C presents the simulation and signal analysis code.

Chapter 2

Biology of Motor Control

While no one knows yet how motor control is actually achieved or what a descending motor command looks like, much is known about the bio-mechanistic processes that underlie execution of motor commands.

There are several descending pathways in the central and peripheral nervous system that form the mechanisms for motor control. These include the lateral and ventral corticospinal tracts, the rubrospinal tract, recticuospinal tracts and tectospinal tract. Full explanations of all these tracts go beyond the scope of this project. The principal goal of this project is to build and investigate models relevant to voluntary isometric co-contracting muscles.

This project therefore focuses on the principal pathway for these motor commands - the lateral cortical-spinal tract. Fibres from this tract are shown to synapse directly with motor and interneurones that control the distal muscles and specifically those that control digits [50]. The lateral corticospinal tract originates primarily in the of the motor and pre-motor cortex and is formed of connections between the upper and lower motoneurones, spinal-interneurones, the muscles being controlled and their sources of afferent information.

2.1 The Cortex

Many areas of the neo-cortex are used to plan and execute movement. It is thought that the cerebellum provides information on movement error, the basal ganglia suppresses unwanted movement and primes the motor-units to initiate movement. Somatosensory input is provided by areas of the Parietal lobe, while the primary and secondary motor cortex provides drive to the motor-units. [50].

Interneurones in the cortex relay information from other neurones and may be the mechanism by which functional assemblies arise in motor control. Brovelli et al [6] showed using Grainger causality how some of the cortical areas were linked in these functional assemblies, showing strong connections between the somatosensory cortex and primary motor cortex, as

well as the posterior parietal cortex.

The focus for this study, the lateral corticospinal tract commences primarily in the motor and pre-motor cortex and as well as in the primary and secondary somatosensory cortices.

The motor cortex is found in Brodmanns' areas 4 & 6 of the frontal lobe and contributes the majority of the descending connections into the cortical-spinal tract. The primary motor cortex (area 4), M1, provides the most concentrated synaptic connections with the the spinal interneurones and motoneurones. It receives input from the secondary motor areas (area 6), primary somatosensory cortex and thalamus amongst others. Areas of M1 are organised into a somatopic map of the body, although this is not quite a one-to-one mapping [50].

Area 6, the secondary motor cortex receives information from the Posterior Parietal lobe and is strongly influenced by the cerebullum and basal ganglia; it is thought that all these areas together participate in the planning of motor acts.

It is believed that the primary motor cortex, M1, represents the final stage of cortical processing before commands are issued to the spinal motoneurones and interneurones [54]. The firing rate of populations of neurones in M1 have been shown to correlate strongly with movement direction and force.

2.2 Motoneurone pool

Lower α motoneurones directly control muscle contraction and are found in clusters in the ventral horn of the spinal cord and in the brain stem. They are spatially located based on the muscles they innervate with those motoneurones driving proximal muscles located nearer the centre of the spinal cord and more distal muscle motoneurones located nearer to the edge of the ventral horn. Because skeletal muscles are not evenly distributed, the lower motoneurones are also unevenly distributed resulting in the size of the ventral horn changing over the length of the spinal column. Hand motoneurones are found in spinal sections C7-C8.

The motoneurones are excited by sensory input from afferent sources, input from spinal interneurones and descending inputs from the upper motoneurones. These inputs diverge extensively across the pool making synaptic connections on a large segment of the population of motoneurones. The primary input for most α motoneurones is from spinal interneurones.

Motoneurone recruitment is shown to follow the size-principle [50]. Smaller motoneurones have larger input resistance and a greater density of current flow across the cell membrane, leading to increased excitability and lower thresholds of firing. Therefore the smallest motoneurones will be recruited first to innverate their muscle fibres. As the drive signal increases, further neurones are recruited based on their size.

A *Motor-unit* is defined by a single α motoneurone and all the muscle fibres it innervates. Together all the α motoneurones which innervate the same muscle form a *motoneurone pool*.

2.3 Muscles

Movement is generated through the contractions and relaxation of muscles. For jointed limbs movement is controlled by groups of antagonistic muscles, with flexor muscles reducing joint angles and extensor muscles increasing them. Muscles may also form co-contracting groups. Therefore, for controlled movement, muscles co-operatively, through the formation of synergies, to facilitate smooth motion.

Each muscle is comprised of many individual contracting extrafusal muscle fibres. An action potential generated by the spiking of a motoneurone causes the release of Acetylocholine (ACh.) at the neurone-muscle fibre synapse. Following the release of ACh. muscle fibre potentials are generated, which travel from the end-plate of the junction to the fibre terminals resulting in a shortening or twitch of the fibre. Each muscle twitch has a contraction and slower, relaxation component. If a subsequent twitch occurs before the fibre has relaxed, then the forces of the twitches combine allowing a higher peak force to be achieved. To achieve a sustained contraction, the muscle fibres must be stimulated by a continuous train of action potentials from the motoneurone that innervates them. When the frequency of firing is high enough, the individual twitches are no longer apparent, resulting in smooth muscle contractions.

Henneman's size principle also states that smaller motoneurones innervate a lower number of muscle fibres, although the ratio of neurones to fibres in a motor-unit varies depending on the muscle. When only a few fibres are innervated then the contraction is weak and can be finely controlled. When lots of fibres are innervated the contractions tend to be more powerful. The type of muscle fibre innervated also varies: white fibres which contract rapidly and powerfully but also fatigue rapidly and red fibres that have the opposite properties. While muscles can contain a mix of fibre types, motor-units only innervate a single type of fibre resulting in the emergence of four main groupings of motor-unit types: slow, fast twitch with intermediate fatigue resistance, fast twitch with fatigue-resistance and fast twitch with fast fatiguing motor-units. Smaller motor-units are more excitable and are a recruited at lower levels of input than the larger units and are typically used to form slow-twitch motor-units with fatigue resistant fibres. The response of a muscle fibre can be altered through muscle activity, developmental changes and disease, which can result in hypertrophy or atrophy of muscle fibres.

The number of active motor-units is proportional to the force the muscle produces and the units' firing frequencies contribute to the regulation of muscle tone. Typically, for isometric contractions of hand muscles, large numbers of slow motor-units are recruited to enable fine muscle control. In experimentally recorded data such units have reported maximum recorded firing rates around 20-25 Hz [41].

2.4 Afferents

Afferent signals relate information about the state of the body and muscles to the central nervous system, providing feedback required for control [6] [50]. There are three principle sources of afferent feedback, also termed proprioceptive feedback, for muscles: primary and secondary spindle receptors and Golgi Tendon Organs. All threes sources relay information about the muscle and its activity to the central and peripheral nervous systems.

Additionally, information is available from secondary exteroceptive and enteroceptive sources including joints and skin receptors. In this project, the focus is on the primary sources of afferent information for isometric contractions: muscle spindles and tendon organs responses.

In the pathways for motor control there are two loops for proprioceptive feedback involving these afferent sources. A short loop, where the output of the receptors' synapses form a local loop in the spinal column and a longer supraspinal loop, involving the pathways to and from the brain. The latency of the shorter loop is around 20ms, and the latency of the longer loop is about 70-90ms. Both pathways are assumed to play an important role in the structuring of motor control signals [23] [6].

2.4.1 Muscle spindles

The primary and secondary spindle afferents are located in specialised structures called muscle spindles that are located in parallel to with a muscle's fibres, within the muscle mass. The spindles are fibrous capsules with a single *Ia* axon and *II* sensory axons wrapping around the intrafusal fibres of the spindle (See Figure 2.1). The spindles form a dedicated unit for the detecting the amount of change and rate of change of muscle length by modulating their discharge rates. The spindle is kept under tension via γ motoneurones which innervate intrafusal fibres in the spindle to keep it contracted relative to the muscle its monitoring.

The *Ia* axon, carrying primary afferent information, forms excitatory synapses upon both the α motoneurones and inhibitory synapses on interneurones of the antagonistic muscle. The axon can form monosynaptic connections with every member of a motoneurone pool and in this way, all motoneurones receive a source of synaptic proprioceptive information. The *II* axons, carrying secondary afferent information, synapse in a similar way but have a slower conduction velocity than the *Ia* axon.

The discharge rates of the axons are closely related to the length of the muscle and for a maintained stretch, they will fire tonically with a discharge proportional to the length of the muscle (see Figure 2.2-a). The output has been shown to be a near linear relationship for a wide range of steady state contractions [39]. There are differences though between the *Ia* and *II* afferents signals (see Figure 2.2-b). Edin et al [16] showed that discharge rates increased during the main part of an isometric contraction with primary afferents increasing more than secondary

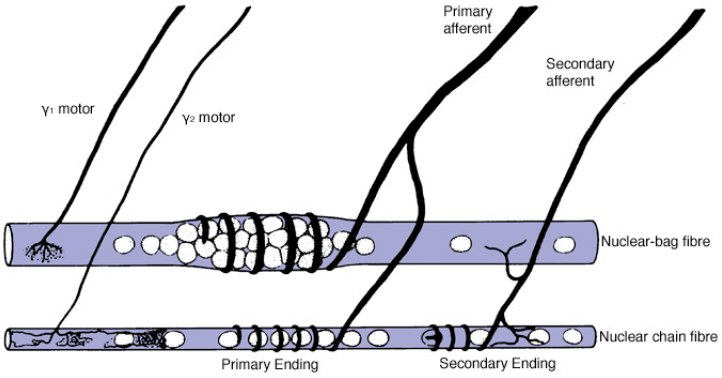

Figure 2.1: Structure of a muscle spindle, adapted from [33]. Shows the central region of a muscle spindle. The spindle contains a mix of nuclear bag and nuclear chain intrafusal fibres (their names reflect how their nuclei are arranged). Typically, each spindle contains a mix of intrafusal fibre types and provides two sources of afferent information.

sources. It is thought that primary spindle afferents encode rate of change information, as they give a dynamic response during a change in muscle length, before returning to signalling the length of the muscle once a stretch is maintained. Secondary sources are reported to have a higher sensitivity to static muscle length than primary with primary sources showing transient falls in discharge rates during the start of a hold phase.

Primary spindle afferents were shown to have more variability in their interspike intervals during voluntary contractions [16] and both sources reached a plateau during the contraction even though the joint torque continued to rise.

The muscle spindle, even at rest, provides a continuous signal to the central and peripheral nervous systems, as long as its held at tension by its γ motoneurones, forming an integral part of the feedback loop that maintains muscle length at a desired value, aiding the planning and execution of movement.

2.4.2 Golgi Tendon Organ

Golgi tendon organs (GTO) measure the tension developed by muscles during contractions caused by active or passive movement. They are another specialised structure and are situated in series with muscle fibres either in or near the muscle-tendon junction (See Figure 2.3). The response of each GTO has a dynamic and static element signalling both the rate of change and overall tension in the fibres its attached.

The output of the GTO is via *Ib* axons which branch and synapse to interneurones in the spinal column. These interneurones typically form inhibitory connections with the innervating motoneurones and prevent the muscle from being overloaded. Through this feedback mecha-

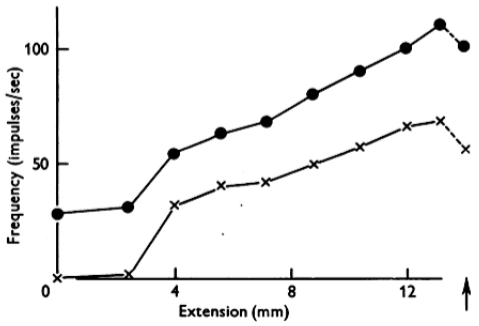

(a) Linear Response

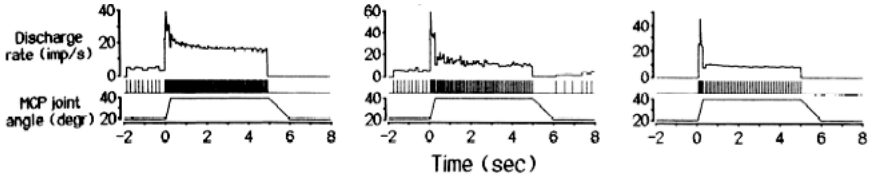

(b) Response to Ramp Stimulus

Figure 2.2: Response of muscle spindles. (a) From [33] Shows discharge versus length of the muscle for secondary endings (with/without ventral root cuts). (b) From [16]. Shows primary afferent response for simple ramp stimulus. Initial discharge is high to encode the rate of length change caused by stimulus before settling to steady-state encoding of length.

nism the GTO helps regulate muscle tension within an optimal range.

Edin & Vallbo [16] recorded the output of muscle spindles and the Golgi tendon organ for a number of tests including an isometric contraction. The GTO, like muscle spindles, is extremely sensitive at small changes in tension resulting in a non-linear overall response. Erin & Valbo also showed that there was no fixed threshold or recruitment level for muscle spindles (See Figure 2.4-a).

However, Crago et al [13] showed that for maintained isometric contractions there is a near straight-line linear relationship between the muscle's tension and the discharge rate of the organ once the GTO begins to respond. Responses ranged between 3.4 and 13 impulses per $S^{-1}N^{-1}$ (See Figure 2.4-b).

2.4.3 Feedback to the Cortex

Proprioceptive information from spindles, tendon organs and mechanoreceptors is feedback to the central nervous system via complex set of ascending pathways. The two principle pathways for proprioceptive information are the Dorsal Column-Medial Lemnsiscus and Trigeminal [50]. These pathways are formed of fast conducting myelinated fibres which pass information through a set of sensory nucleus in the spinal cord or brain stem, into the Medial-Lemniscus which forms synapses in the lateral and medial nucleus of Thalamus. From the

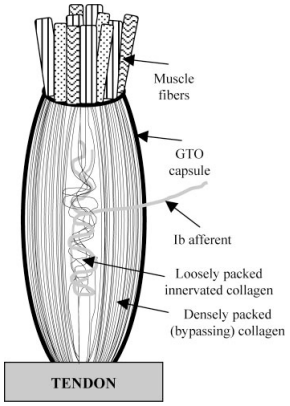

Figure 2.3: From [40]. Structure of the Golgi tendon organ. Tendon organs are in series with muscle fibres and the tendon they attach to. A rough estimate is that there are 10-20 muscle fibres connecting to each GTO. Each muscle has multiple GTOs measuring tension [39] the effect of which is to provide a sample of the overall muscle tension.

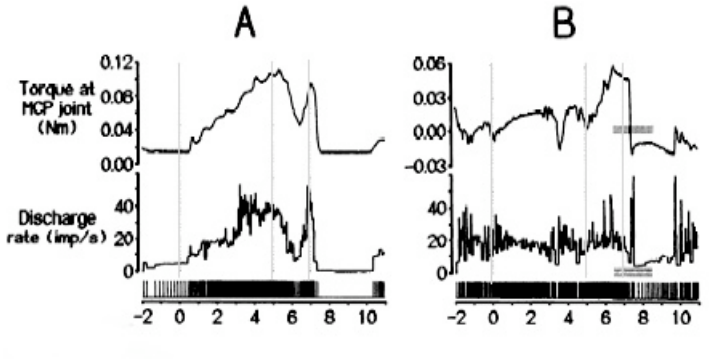

(a) GTO response variations

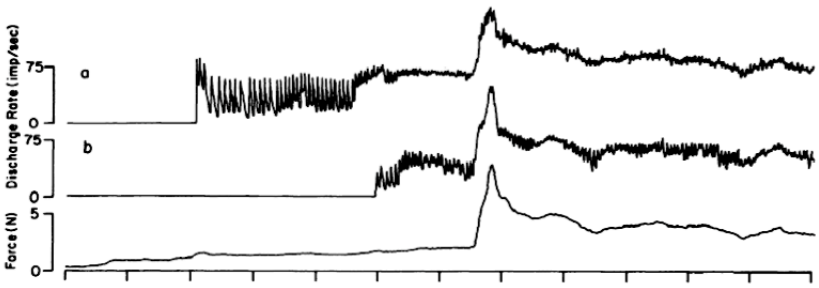

(b) Response to Ramp Stimulus

Figure 2.4: Response of GTO. (a) From [16]. Shows the response of two different GTOs and the variation in response. (b) From [13]. Shows the discharge rate of two GTO recruited with different thresholds.

Thalamus afferent signals are then projected to differing locations in the primary somatosensory cortex, depending on the location and source of information.

Further connections and inputs are also received and created at all levels in the ascending pathways. The route taken by afferent information is affected by the position of the proprioceptive organ in the body. Information from the face, arms and legs all take a slightly different pathways with differing connections. These connections can involve a wide variety of neural structures including Clarke's columns in the spinal cord, the Z nucleus and cerebellum.

Chapter 3

Model

Experimental research has shown that motor-unit activity is controlled not only by a central drive to the motor-units, but is also by motoneurone adaptation and afferent feedback from the active muscles [8] [23]. To explore the relationship between these components and the production of synchronous common drive, a new model of the the corticospinal projection is presented, in which only the central cortiospinal pathways are considered. This projection model has the following principal components: simulated input from other cortical areas, a cortical sheet of upper motoneurones, a sophisticated synaptic channel model, a spinal cord section consisting of α motoneurones and interneurones, simulated twitch muscles and output signals (See Figure 3.1).

3.1 Input

Input to the cortical sheet is in the form of a driving signal from a Poisson point process neurone, which makes synaptic connections with a number of the excitatory neurones in the upper-sheet, introducing stimulating firing at a tuneable frequency for neurones in the sheet. The temporal distribution of cortical spikes has been shown to approximate that derived from a Poisson process under numerous experimental conditions [15]. While it is biologically implausible for a single-cell to be the source of common drive, its position in the model is of synchronising drive from a population of neurones elsewhere in the cortex [5].

Other studies [11] have used an Ornstein-Uhlenbeck process to generate a randomly fluctuating current or simulations of Thalamus rhythms [32] to provide a drive signal. All such models are potentially plausible as there is no clear understanding of what a 'motor-signal' looks like. However, this common input model provides a simple method of tuning the output of the cortical sheet.

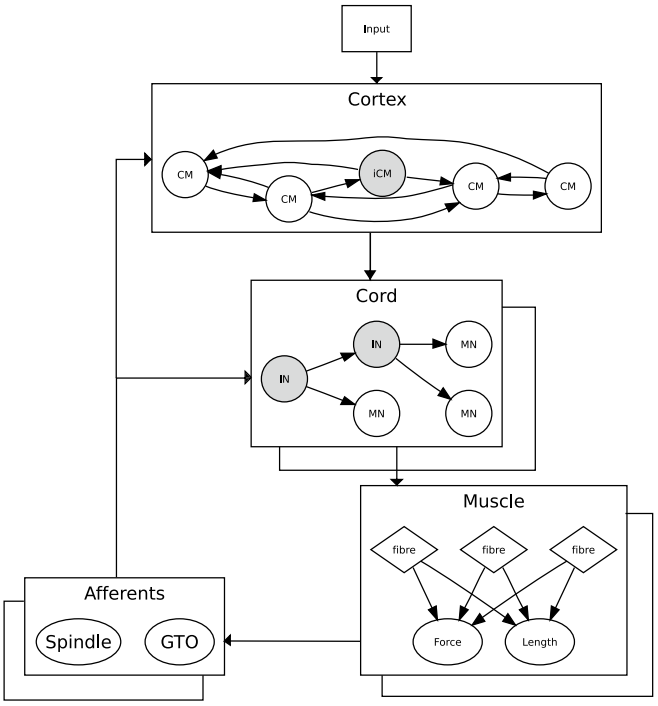

Figure 3.1: Overview of the simulation model. Input connects to a sheet of cortical neurones. The cortical neurones (CM) have a given level of inhibition and connectivity. Descending connections to the lower motoneurones are parameterisable and can be simulated on one-to-many through to one-to-one connections with the motoneurone pool. Motoneurones (MN) inerverate motor-units which activate muscle fibres. Afferent information about the activity in the muscle is fedback into the motoneurone pool and cortex via Golgoi tendon organs and muscle spindles.

3.2 Sheet of upper motoneurones (β)

To approximate the cortical layers involved in voluntary movement requires modelling connected collections of neurones. A review of the literature reveals a plethora of neurone models ranging from basic integrate-fire neurones through to mathematically complex models including Hodgkin-Huxley based approaches[15] [22] [30]. To be useable, any complex simulation has conflicting demands because it needs to capture the rich dynamics of neuronal activity while remaining computationally tractable. After a review, three neurone models were evaluated based on their prior use in simulating cortical models with some complexity: leaky integrate and fire neurones with spike-frequency-dependent adaptation [51], Izhikevich's neurone model [30] and Ashby & Zimm's neurones [1]. Izhikevich neurones were selected due to their computational efficiency and the ability to model the spiking and bursting behaviour of many known cortical cells [30]. Simulations involving thousands of these neurones are possible in reasonable time periods [32]. Section 3.2.1 discusses this model in detail.

An approximation of the primary motor cortex (PMC) is constructed, simulating the upper motoneurones, which are responsible for transmitting motor command information for voluntary movement, and other areas of the PMC [50]. The upper sheet of neurones are randomly assigned connections based on a user definable connectivity parameter, rather than following a two-dimensional [45] or three dimensional sphere [32] assignment strategy. A spatial arrangement is instead simulated by the assignment of random delays. Neurones are connected using the synaptic connection model discussed in Section 3.3.

The level of inhibition in the sheet is also parameterised allowing the information structuring dynamics of the sheet to be explored. Cortex studies have shown the ratio of excitatory to inhibitory connections to be approximately a 4:1 ratio [50] and simulation results have shown that levels of inhibition above 15% are required for oscillatory behaviour [45].

Different connectivity models between the sheet and motoneurone pools are possible allowing exploration of the dynamics of cortical-motoneurone projections. One-to-one cortical motoneurone projections can be studied, as well one-to-many and one-to-all projections of Baker [5] with parameterised connectivity and delays.

3.2.1 Cortical neurone model

Each neurone in the cortical sheet uses Izhikevich's neurone model [30], where the membrane potential of a neurone is described by two ordinary differential equations (3.1) and (3.2).

$$\frac{dv}{dt} = 0.04v^2 + 5v + 140 - u + I \tag{3.1}$$

$$\frac{du}{dt} = a(bv - u) \tag{3.2}$$

Where v represents the membrane potential of the neurone, u represents a membrane recovery variable, which accounts for the activation of potassium channels and the closure of calcium channels and I is the injected current. The dimensionless variable a controls the time scale of the recovery variable u, b describes the sensitivity of u to sub-threshold[1] variations in the membrane potential and d controls the after-spike reset of the recovery variable.

When a neurone's membrane potential reaches the peak of the action potential (AP) spike it is then reset based on (3.3), where v_{max} is the maximum height of the spike (typically 30mV) and c is the after-spike reset value of the mebrane potential (typically -65mV). The parameters used in (3.1) are fitted such that v has a mV scale and t has a mS scale.

$$\text{if } u \geq v_{max}, \text{ then } \begin{cases} v \leftarrow c \\ u \leftarrow u + d \end{cases} \tag{3.3}$$

The choice of the parameters a, b, c and d can result in a wide range of firing patterns and can be tuned to match recorded firing patterns of known cortical neurone types [31]. Two types of cortical neurones are used in the sheet: regular spiking (RS) for excitatory neurones and fast-spiking (FS) for inhibitory based on the parameters in Table 3.1.

Parameter	**RS**	**FF**
a	0.02	0.1
b	0.2	0.2
c	-65	-65
d	8	2

Table 3.1: Typical parameter values for RS and FS cortical neurones.

A further desirable property of the Izhikevich neurone model is that there is no fixed firing threshold and therefore the neurones can show voltage adaptation. Figure 3.2 shows the models response for an injected step current of 10nA, simulated with a time step of 0.1ms. Regular spiking neurones mimic the response of the majority of neurones in the cortex and display voltage adaptation. Increasing the injected current results in increased firing, but it is constrained by the large after-hyperpolarization period. The fast spiking neurones fire with a high frequency without displaying adaptation due to their much faster recovery period.

3.3 Synaptic channels

An action potential from a spiking neurone propagates to the pre-synaptic terminal causing neurotransmitter release and leading to a post-synaptic potential (PSP). The model follows the

[1] Variations in the membrane potential that stay below the firing threshold.

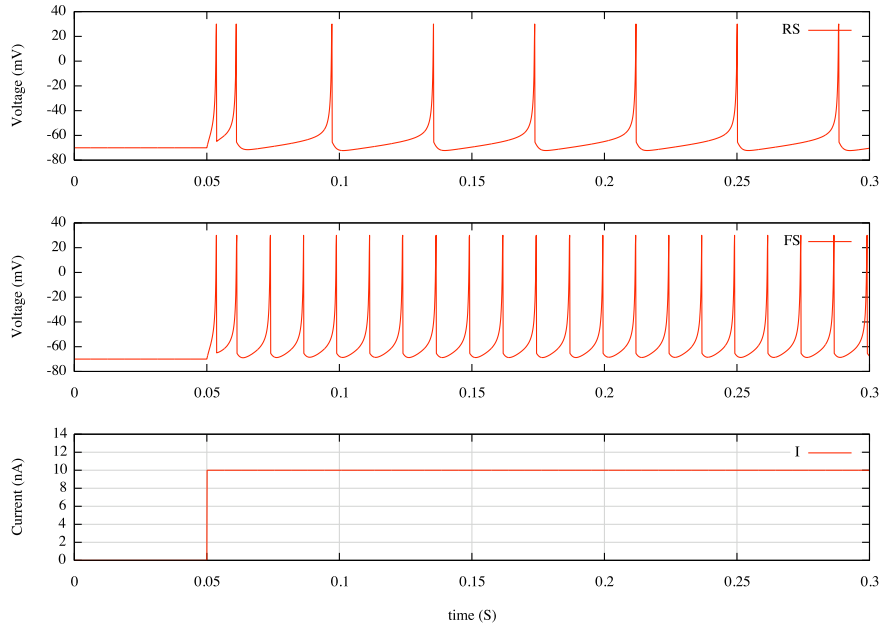

Figure 3.2: Regular and Fast spiking models' response to injected step current. Top: shows a regular spiking neurone. Middle: response of a fast spiking model neurone used for inhibitory interneurones. Bottom: injected current in nA.

basic view that an excitatory PSPs (E_{psp}) depolarize a neurone's membrane and inhibitory PSPs (I_{PSP}) hyperpolarize it [22].

Kudela et al's [36] [37] model of synaptic channels is used to model connections between all neurones. A small modification is made to ensure that time courses of PSPs match the observed bevahiour of PSPs *in viro*. The shape of a PSP depends on the connection type and the membrane potential of the post-synaptic neurone. An I_{psp} arriving while the neurone is at rest will have little effect of the membrane potential, while one arriving while the neurone is depolarising will have a much larger effect. Additionally, when the neurone is hyperpolarised the sign of the I_{PSP} will be reversed.The effect of an E_{PSP} depends significantly less on the membrane's polarization state and consequently, the amplitude changes of the induced current are much less pronounced [22].

Each synaptic channel is described by equations (3.4 - 3.7). The contribution of each synaptic input's current is summed for all inhibitory and excitatory input synapses (3.4). The contribution of each channel type is given by the alpha functions in (3.5) and (3.6), where w is the synaptic weight of the channel, g is its synaptic conductance, τ is the synaptic delay and E_{syn} is the synaptic reverse potential of the channel.

$$I_{psp} = \sum_{j=1}^{N_I} I_{ipsp} + \sum_{j=1}^{N_E} I_{epsp} \tag{3.4}$$

$$I_{ipsp} = w.g(t-\tau)(E_{syn} - V) \tag{3.5}$$

$$I_{epsp} = w.g(t-\tau)(|E_{syn} - V|) \tag{3.6}$$

The synaptic conductance, g is generated via summation over the N last pre-synaptic action potentials (3.7), where Δt is the elapsed time since the action potential arrived and T_d and T_o are the decay and onset time parameters of a post-synaptic potential. Manipulation of T_d and T_o allow alteration of the time course of the evoked PSPs. N is dependent on the decay parameter, T_d and typically provides a summation window ranging over 15-20ms.

$$g(t) = g_{max} \sum_{i=1}^{N} (e^{\frac{-\Delta t}{T_d}} - e^{\frac{-\Delta t}{T_o}}) \tag{3.7}$$

Typical parameters used during simulation are given in Table 3.2. g_{max} is manipulated so that the peak contribution of the channel is $\approxeq$ 1.2 nA

Parameter	Description	Value	Unit	ref
E_{syn_e}	Excitatory synaptic reverse potential	10.0	mV	[36]
E_{syn_i}	Inhibitory synaptic reverse potential	-72.0	mV	[36]
T_d	Time decay parameter	3.0	mS	[36]
T_o	Time onset parameter	0.5	mS	[36]
g_{max}	Synaptic conductance constant	0.0066 - 0.028	mS/cm^2	[36] [5]
W	Synaptic connection weight	0.0 - 1.0	-	

Table 3.2: Synaptic channel parameters.

3.4 Lower α motoneurones pool

Local circuits of interneurones and α motoneurones are simulated using Powers' motoneurone model [47], which is a basic threshold-crossing model with simulated ion channels. This model has been used extensively by Baker [4] [5] and others [38] [43] in motoneurone pool modelling and captures the discharge behaviour of cat motoneurones [47] while remaining computationally efficient.

3.4.1 Motoneurone model

Powers' motoneurone model is single compartment model with five simulated channels: a leakage channel, fast and slow potassium channels and low and high threshold calcium channels [47].

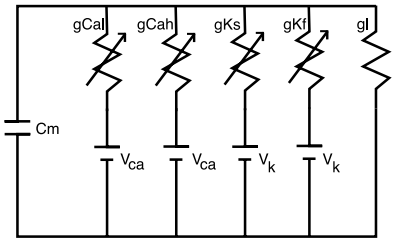

Figure 3.3: Equivalent circuit for Powers' model. The model is represented as an isopotential patch of membrane with four active conductances and passive leakage and capacitance properties. From [47].

The membrane potential, V of each motoneurone, with reference to its resting potential is described by (3.8), where C is the membrane capacitance, g is the conductance and I the input current. g_l is the conductance of the leakage channel and i indexes the slow potassium, fast potassium, low-theshold calcium and high-threshold calcium ionic channels respectively.

$$\frac{dV}{dt} = \frac{1}{C}[I - \sum_{i=1}^{4} g_i.(V - V_{eq_i}) - g_l V] \tag{3.8}$$

The relationship between membrane voltage and the ionic conductances is given by (3.9), where g_{max} is the maximum conductance and $a_i(V)$ is the activation function, describing the relative conductance, which varies from 0 to 1.

$$g_i = g_{max_i}.a_i(V) \tag{3.9}$$

The steady state relationship between the membrane potential and the channel's conductance is described by an S-shaped curve (3.10). V_{h_i} is the voltage for half-activation of the conductance channel i and s_i is a constant, which effects the gradient of the voltage-conductance curve for the channel. (Figure A.1 shows typical activation values for the ionic channels in this model.)

$$a_{\infty_i}(V) = \frac{1}{1 + exp(\frac{V_{h_i} - V}{s_i})} \tag{3.10}$$

The activation function, $a_i(V)$ therefore approaches the steady state conductance value, as described in (3.11), where τ_i is a time constant equal to τ_{max} between APs and τ_{min} during APs.

$$\frac{d}{dt}a_i(V) = -\frac{1}{\tau_i}[a_i(V) - a_{\infty_i}(V)] \tag{3.11}$$

In vivo motoneurones show adaptation, where the initial firing changes in response to the level of stimulus. The rate is higher at the onset of stimulus than after a series of spikes and the slow K^+ channel is considered the primary contributing factor for this adaptation [43][48].

Second order kinetics are added to the model by changing the conductance equation for this channel from (3.9) to (3.12).

$$g_{Ks} = g_{max}.a_{Ks}^2(V) \tag{3.12}$$

Action potentials are generated for a motoneurone when its membrane potential crosses the voltage threshold. A voltage impulse of 1ms duration is then generated, provided that the time since the last action potential is $>$ 2ms. This restriction limits the maximum firing rate of the model to 500 impulses a second. However this is much higher than motoneurone firings recorded experimentally, which rarely exceed 100 impulses a second [47].

Table 3.3 shows the ionic conductance parameters used for all motoneurones.

Channel	g_{max} (μS)	V_h (mV)	V_{eq} (mV)	s (mV^{-1})	T_{max} (ms)	T_{min} (mV)
Slow potassium	3.16	28	-15	10	36	1.4
Fast potassium	2.6	45	-15	4	2	1
Low-threshold calcium	0.46	16.5	150	2.5	20	20
High-threshold calcium	0.1	28	150	3.5	4	2

Table 3.3: Ionic channel parameters taken from Powers [47]

3.4.1.1 Variable voltage threshold

The firing threshold of motoneurons has been shown to vary in response to input current and membrane potential[8] [47] [48]. In addition to the second order kinetics already described, an extended variable voltage model is also used, where the firing threshold at each time step is computed using (3.13) [43].

$$v_{thresh}(t) = v_{thresh_0} + v_{thresh_I}(t) + v_{thresh_M}(t) \tag{3.13}$$

Where v_{thresh_0} is the minimum threshold value, v_{thresh_I} is the increase to the threshold due to the driving current and v_{thresh_M} is the increase due to the membrane potential (3.14).

$$v_{thresh_M} = a(V).\bar{v_{thresh_M}} \tag{3.14}$$

Where $a(V)$ is the activation function seen previously (3.11) using the parameters from Table 3.4 and $\bar{v_{thresh_M}}$ is the maximum value of the voltage dependent increase.

The increase in threshold due to driving current, v_{thresh_I}, is calculated using (3.15 - 3.17), where I is the driving current caused by PSPs and any injected current.

$$I = I_{PSP} + I_{input} \tag{3.15}$$

$$v_{thresh_I\infty}(I) = \begin{cases} 0, & \text{if } I - I_R < 0 \\ c(I - I_R) & \text{otherwise} \end{cases} \tag{3.16}$$

Where I_R, the rheobase, is approximated by $I_R = g_{leak} \cdot v_{thresh_0}$.

$$\frac{d}{dt} v_{thresh_I}(t) = -\frac{1}{c_\tau}[v_{thresh_I} - v_{thresh_I\infty}(I)] \tag{3.17}$$

For all the neurones in the motoneurone pool, the parameters from Table 3.4 are used in calculating the voltage-threshold. v_{thresh_0}, the base voltage threshold is dependent on the motor-unit type and has been shown to vary considerably, ranging from 4.0 to 13.74 mV [38].

Parameter	Description	Value	Unit	References
V_h	Activation function's half activation voltage	18	mV	[38]
s	Voltage dependence constant	5	mV^{-1}	[38]
τ_{max}	Activation function's time constant between APs	2	ms	[38]
τ_{min}	Activation function's time constant during APs	0.5	ms	[38]
v_{thresh_M}	Max voltage threshold increase	12	mV	[47]
c	Rate of increase	0.12	mV/nA	[47]
c_τ	Time constant	50	ms	[47]

Table 3.4: Common variable-threshold parameters

3.4.1.2 Motoneurone pool

The model follows Baker's example of motoneurone pool [5] with a variable number of motoneurones and interneurons. The size of the pool is parameterisable, though typically pools are formed of 100 neurones, which is comparable to similar studies [20] [38] [53] and biology [50], with a smaller number of interneurones. Each motoneurone is assigned the a set of common values (Table 3.3 and 3.4). Other values are assigned based on the size-principal. Input conductance, membrane capacitance and voltage threshold increase exponentially from the smallest, earliest recruited neurone (1) to the largest, last to be recruited neurone (100). Values for input conductance, motoneurone membrane capacictance and initial voltage threshold were assigned based on the ranges shown in Table 3.4.1.2 and Figure 3.4 shows the responses of motoneurones 1, 50 and 100 to 100ms of injected 20nA current.

Noise is also added to the membrane potentials of all the motoneurones drawn from independent Gaussian distributions, with a standard deviation of 2mV and a time constant of 4ms [5] [7] [38].

Parameter	Description	Range	Mean	Unit	References
g_l	Input conductance	0.17-1.26	0.40	μS	[38]
C	Membrane Capacitance	6.50-9.80	8.17	nF	[57]
V_{thresh_0}	Initial voltage threshold	4.00-13.74	7.12	mV	[38]

Table 3.5: Variable parameters for motoneurone pool

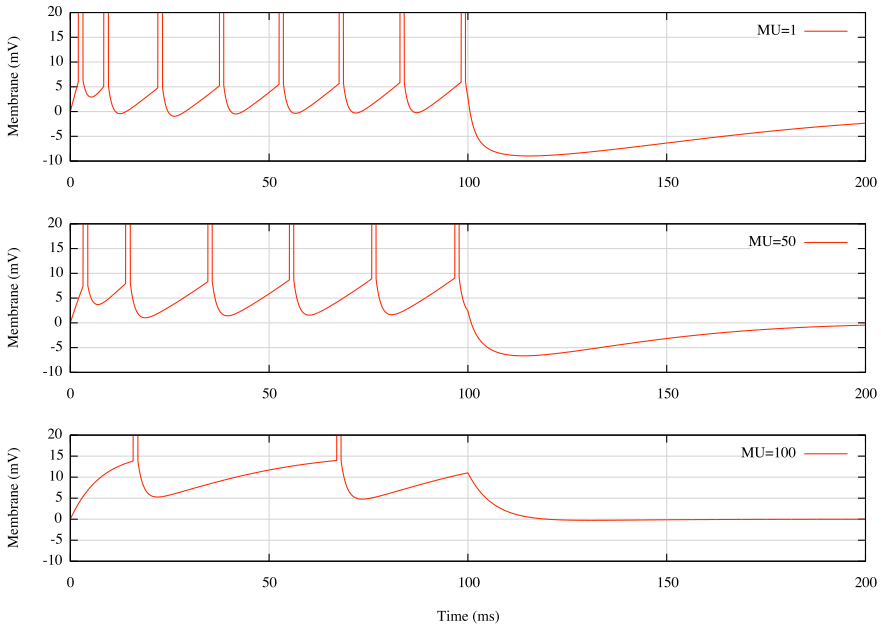

Figure 3.4: Motoneurone pool responses to injected current.

3.4.2 Interneurones

Much of the information received by the motoneurone pool is from synapse connections from the spinal interneruons [50]. In this study a tuneable pool of interneurones is modelled, which form mono-synaptic connections on every motoneurone. The interneurones are modelled as fast spiking Izhievich neurones (Section 3.2.1) following the procedure in Section 3.2.1. The source of connections to the spinal interneurones is variable, but all receive information from the Golgi tendon organs, establishing a negative feedback loop.

3.5 Muscle

Muscle force produced by each motor-unit is simulated using the model of Fuglevand, Winter and Palta [20]. In this model, motor-unit twitch force is approximated by a critically damped second-order system with a non-linear force behaviour.

Each motor-unit is assigned a peak twitch force and twitch contraction time. An action potential generated by a motor-unit generates a twitch force in the simulated muscle, which then is scaled by the instantaneous interspike-interval (IIS) of the motor-unit to allow the muscle force to vary as function of the firing rate and match experimental data [20] [38].

The force produced at time t by the ith motoneurone is given by (3.18), where g_i is the IIS scaling factor, P_i is the peak twitch force of the motoneurone and T_i is the twitch contraction time (the time taken for the force produced to reach P_i).

$$f_i(t) = g_i \frac{P_i.t}{T_i} e^{1-(\frac{t}{T_i})} \tag{3.18}$$

The non-linear force behaviour of model occurs by allowing the gain, g_i to vary as function of the firing rate (3.20). However, g_i is assumed to be constant at low firing rates and its behaviour is toggled by (3.19), where ISI_i is the instantaneous interspike-interval of the ith motoneurone, giving a normalized stimulus rate.

$$N_i = \frac{T_i}{ISI_i} \tag{3.19}$$

If the normalized firing rate, N_i is ≤ 4 then gain is constant and linear. Above this threshold, the gain follows a sigmoid non-linear form which matches experimental data (See [20] for further details).

$$g_i = \begin{cases} 1, & \text{if } N_i \leq 4.0 \\ (1/N_i)x(1-e^{-2(N_i^3)}) & \text{otherwise} \end{cases} \tag{3.20}$$

Force response to a train of of discharges is calculated by summing the response to each individual impulse response (3.21) The signals for each motor-unit are then simply summed

together to provide an instantaneous total muscle force signal (3.22) based on the assumption that the motor-units are independent of each other.

$$F_i(t) = \sum_{j=1}^{k} f_{ij}(t - t_{ij}) \text{ where } t - t_{ij} \geq 0 \tag{3.21}$$

$$F(t) = \sum_{i=1}^{n} F_i(t) \tag{3.22}$$

Values for motor-unit peak twitch force and contraction time are assigned based on experimental data (Table 3.5). There have been many studies all with slightly varying values. Carpentier et al [8] reported motor-unit forces between 1-158mN and time-to-peak values of between 25-105ms for isometric contractions of the first dorsal interossous muscle. Gossen et al. [25] reported similar figures of 1-75 mN and 42-76ms for force and contraction times respectively. Following this experimental data, the values used by Lowery [38] are applied, as they correlate well with the available experimental data and sit within the middle range. Peak twitch force is assigned to each motoneurone in an exponentially increasing series and time-to-peak contraction is assigned in an exponentially decreasing series, with the smallest motor-unit having the smallest and slowest twitch force and the largest motor-unit having the largest and fastest.

Parameter	Description	Units	Range	References
P_i	Peak twitch force	mN	1.04-80.00	[38]
T_i	Time to peak twitch force	mS	25.0-90.0	[8], [38], [53]

Table 3.6: Model muscle parameters

Figure 3.5 shows a plot of twitch forces as a function of contraction time for the entire motoneurone pool. Smaller motor-units are activated early, but have both slow contraction times and low twitch force values. More than half of all motor-units under this assignment generate twitch forces below 10 mN.

3.6 Afferent signals

Riddle and Baker [52] showed that afferent feedback is involved in the gensis of coherence and plays an important role in aiding the performance of motor tasks. During isometric contraction, the model considers two sources of afferent feedback: the Golgi tendon organ and muscle spindles as these are directly related to muscle tone.

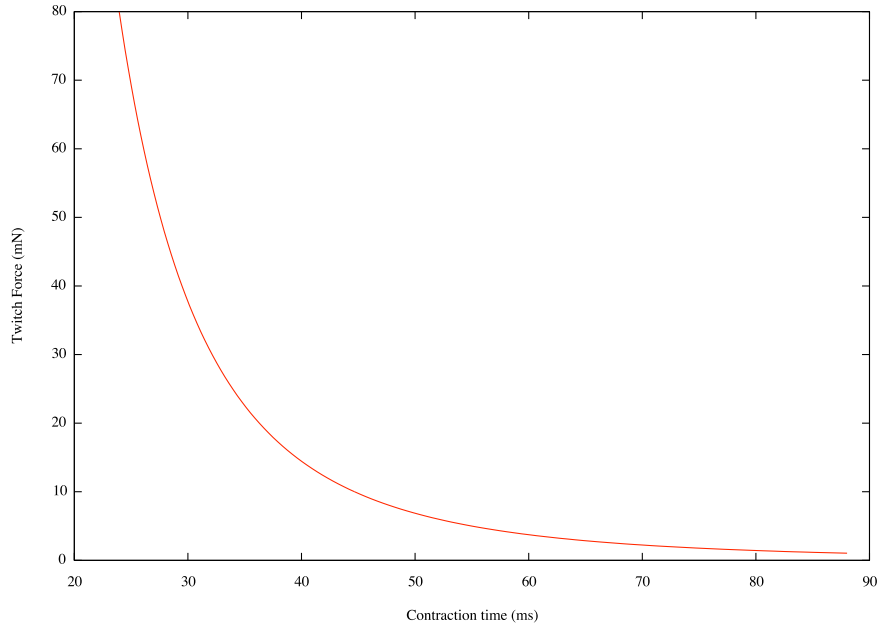

Figure 3.5: Twitch parameter assignment for motoneurone pool. Motor-unit 100 is at the far left and motor-unit 1 is at the far right of the distribution.

.

Golgi tendon organ (GTO)

The Golgi tendon organ is the principle source of afferent feedback for isometric contractions giving both information on the rate of change and the overall amount of tension in the muscle. There have been a few models of the GTO but most are computationally and biologically complex; [40] is one such example.

Because this study is focused on steady-state isometric contractions, the aggregate output of the GTOs in the muscle is modelled as simple Poisson point process, where the instantaneous firing rate is defined by (3.23), where f is the force of the muscle, Δ is the drawn from the range reported by Crago et al [13] and $\xi(E)$ is a source of noise drawn from a Gaussian distribution with mean of zero and a standard deviation of 0.5 (both parameterizable).

$$Imp = \begin{cases} 0, & \text{if } f \leq \mathrm{f}_{thresh} \\ \Delta f + C.f + \xi(E) & \text{otherwise} \end{cases} \tag{3.23}$$

Each GTO is given its own threshold firing rate, f_{thresh}, which is typically set at 0.5% of the maximum force of the muscle.

Muscle spindles

Muscle spindles provide constant feedback to the motoneurone pool and cortex. However, during isometric contractions there is no length information to encode because there is no

movement. It is therefore assumed that the spindle provides a low level of constant output [16]. Like the tendon organ, there are multiple muscle spindles reporting information and in this model their activity is summed into an aggregate unit source which is weighted accordingly.

Therefore as with the GTO, the force value is used to set the ISI of a Poisson spike train 3.24, where $\xi(E)$ is drawn from a Gaussian distribution with a mean of 0 and a standard deviation of 0.5 and *Base* is a steady state firing rate drawn from experimental data [13] [16].

$$ISI = Base + D.f + \xi(E) \tag{3.24}$$

This forms a crude approximation of a primary spindle afferent based on the observation that 'individual afferents showed stereotypical response profiles to repeated isometric contractions' [16]. This model approximates the signal of more complex models during the hold section of a ramp and hold contraction [49] and provides an appropriate first approximation in the absence of muscle length information.

3.7 Simulated EEG and EMG output

Both simulated Electroencephalogram (EEG) and Electromyogram (EMG) outputs are provided by the model to allow direct comparison with other simulated [20] [43] [56] or experimental studies [3] [23] [18].

3.7.1 Simulated EEG

EEG is a recording of electrical activity on the surface of the surface of the scalp representing a summation of many thousands of PSPs invoked in the input to cortical neurones. To be able to compare EEG/EMG studies with output in the model, a record of activity in the cortical sheet is required. A Pseudo EEG (pEEG) signal is simulated by summing the activity of all neurones in the cortical sheet and then low-pass filtering the signal. This gives a simple measure of the a spatio-temporal average activity in the sheet, and while not biologically plausible, it gives a strong signal useful for comparison.

3.7.2 Simulated EMG

EMG recordings capture the electrical fields generated by propagating currents invoked during muscle contraction. To provide direct comparison with the EMG studies of Farmer et al [18], Hockensmith et al [29] and others, the action potentials for each motor-unit need to be converted into motor-unit action potentials, which can then be summed to simulate surface EMGs [5].

In this model, Fuglevand's model of surface EMGs is utilized to achieve EMG simulation [20]. A pseudo EMG signal is created based on the spiking times of the motor-units in the

simulator. For each action potential, depolarisation of a segment of muscle fibre occurs which represents the potential distribution detected in EMGs. The depolarisation travels travels along the fibre in the form of propagating action potential. Motor-unit action potentials are assumed to be the sum of their constituent fibre potentials. The model uses a dipole model of the transmembrane current to simulate individual fibre potentials

A three-dimensional muscle volume is created to simulate MUPs, which includes the effects of anisotropic muscle conductance, innerveration zone length, electrode size and placement and propogation velocity. The muscle volume is assigned based on the number fibres within the muscle, assuming all fibres have the same diameter (56μm). The muscle volume is then divided into a number of isopotential layers, each 0.5mm wide.

Motor-unit territories are then placed randomly within the muscle volume (See Figure 3.6). The assumption is made that all fibre potentials in each isopotential layer cause similar fibre potentials at the electrode. A further assumption that each motor-unit innverates a number of fibres linearly proportional to the motoneurones size and that the density of fibres in the muscle is constant (20 unit fibres mm^2) is made. The smallest motor-unit stimulates the smallest number of fibres and has the smallest territory in the muscle.

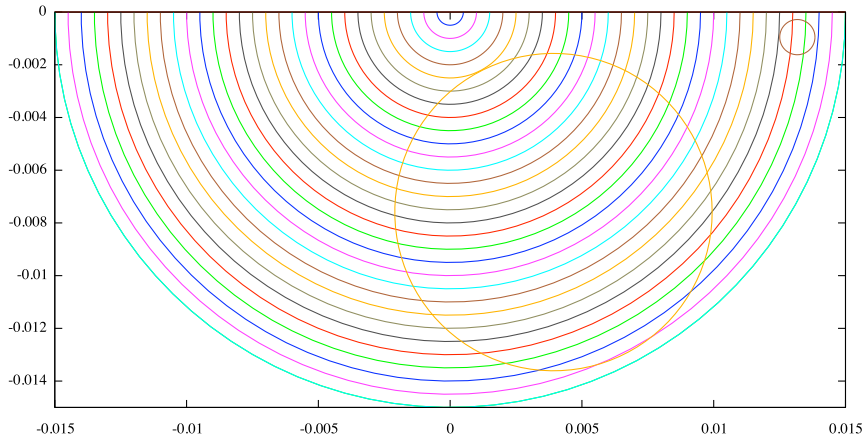

Figure 3.6: Motor-unit area assignment in simulated muscle. Muscle radius is 15mm with isopotential areas are created every 0.5mm. Two motor-unit territories are displayed (as circles): one small motor-unit which stimulates 28 fibres and has a territory diameter of 1.34mm and a larger motor-unit, encompassing some 2278 fibres with a territory of 12.05mm. The electrode is assumed to be placed directly over the centre of the hemisphere.

Once muscle-unit territories have been assigned, the area of interesction of each muscle

unit and isopotential layer is generated. From this area and the density of muscle fibres in the motor-unit, the number of fibres in each layer is calculated. Potentials are then be calculated using infinite volume conductor line source model. The action potentials originate in the end-plate (assumed to be exactly halfway along the fibres length) and propagates axially with a constant velocity. The potential at a point electrode in a single fibre is generated using the following equations 3.25 - 3.30, which represent a pair of dipole current sources moving away from the innervation point, propagating current along the muscle fibre.

$$\Phi(t) = \frac{I}{4\pi\sigma}[\frac{1}{r1} - \frac{1}{r2} - \frac{1}{r3} + \frac{1}{r4}] \tag{3.25}$$

$$\frac{1}{r1} = \frac{1}{\sqrt{r_f^2.\sigma_{ratio} + (v.t - z_e)^2}} \tag{3.26}$$

$$\frac{1}{r2} = \frac{1}{\sqrt{r_f^2.\sigma_{ratio} + (v.t - z_e + b)^2}} \tag{3.27}$$

$$\frac{1}{r3} = \frac{1}{\sqrt{r_f^2.\sigma_{ratio} + (-v.t - z_e)^2}} \tag{3.28}$$

$$\frac{1}{r4} = \frac{1}{\sqrt{r_f^2.\sigma_{ratio} + (-v.t - z_e - b)^2}} \tag{3.29}$$

$$\sigma_{ratio} = \frac{\sigma_z}{\sigma_r} \tag{3.30}$$

Where the muscle fibre parameters are shown in Table 3.7. These equations are used to simulate a potential at the centre of an isopotential layer. The individual MFP is then multiplied by the number of motor-unit fibres in that isopotential layer. The potential for each layer is then summed to give the MUAP. MUAPs can then be combined to form the surface EMG.

The placement of electrodes has a noticeable effect on the EMG recorded. The model records EMG with two point electrodes aligned with directly over the fibre, they are separated

Parameter	**Description)**	**Value**	**Units**
I	Dipole current	388	μA
b	Dipole spacing	1	mm
σ_r	Radial conductivity	0.063	mhos/m
σ_z	Longitudinal conductivity	0.33	mhos/m
v	Conduction velocity	2-5	m/s
z_e	End-plate electrode distance	40	mm

Table 3.7: Muscle fibre action potential parameters [21] [56]

in the z-direction (parallel to the fibre) and assumed to be 11mm apart and are additionally separated from the muscle by an additional subcutaneous layer of 1.5mm.

A modified form of the current source is simulated to overcome an issue with the assumptions that currents ‘spring-up’ instantaneously when the fibre is depolarised (See Appendix A.4 for details).

Chapter 4

Simulation Results

The strength of this simulation model is that it supports a large number of parameterisable settings that enables the exploration of multiple facets of the corticospinal projection, providing multiple sources of data unavailable from pure biological research.

The results presented in this chapter are presented as illustrative examples of both the strengths and weaknesses of the current simulation implementation and not as exhaustive representations of the potential application of the model. The following results are presented as evidence of the richness of the simulation and its ability to produce results comparable with those presented by Farmer et al [18], while providing a plethora of additional information to aid in the understanding and interpretation of those results.

4.1 Data analysis

The model can produce a wide variety of data from spike trains, interspike interval recordings, spike time information, membrane potentials, synaptic channel currents, pseudo EEG (pEEG) and EMG signals.

The pEEG and EMG signals are low pass filtered, rectified and normalised to have unit variance [18] before being Fast Fourier transformed. Further frequency and time analysis is then applied, following the approach outlined by Halliday et al [27] [26], to generate coherence and correlation information between the two time series.

Coherence in the signals is computed by first generating the auto-spectra of each signal and their cross-spectra. From these spectras, coherence is then estimated from the magnitude square of the cross-spectra and normalised by the product of the auto-spectra. This coherence measure gives an estimate of how much activity in one time series can be predicted in the activity of a second time series. In the case of EEG-EMG analysis, the pEEG signals are set to be the reference and EMG is the response signal. For EMG-EMG analysis, one simulated muscle's EMG is arbitrarily defined as the reference signal because there is no spatial relationship

between them.

Correlation of the signals in the time domain is computed through estimating the cumulant density function. For two unrelated signals the cumulant estimate should be zero. When the signals have a given relationship, the cumulant estimate will be non-zero at given time-lag.

For both groups of signals, 95% confidence limits are generated, which indicate the significance of the relationship by indicating the level above which this result is likely to be a true for a wider population of samples [28] [18].

Analysis of data was performed principally using Neurospec 1.0 Matlab library [26] and Matlab's FFT functions. The Neurospec package has been used for a numerous studies including Farmer et al. [18].

4.1.1 Maximum voluntary contractions of muscles

To study isometric contractions, the maximum voluntary contraction (MVC) force of a muscle must be measured to provide a benchmark for comparison. By measuring the maximum contraction force available, studies can ensure that the actual contractions observed are significantly below this peak, avoiding muscle fatigue effects. Using the model motoneurones in the projection simulation the MVC force available was calculated by introducing a steadily increasing drive current to all the motoneurones. The peak force recorded was defined as the MVC (see Figure 4.1).

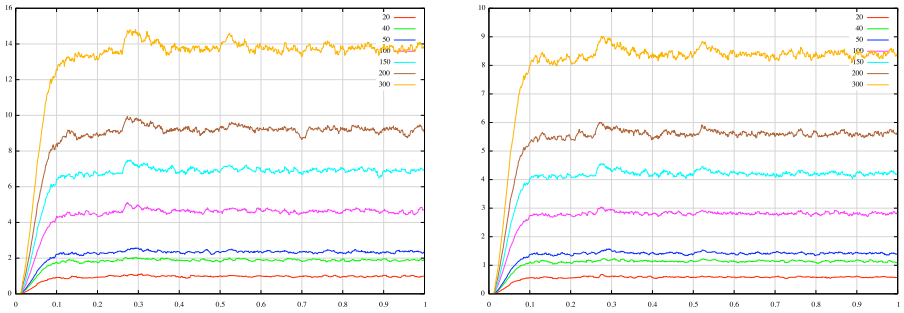

(a) MVC of Simulated Muscle with 100 motoneurones

(b) MVC of simulated muscle with 50% reduction in max peak twitch force and contraction time

Figure 4.1: Steady state MVC values for increasing motoneurone pool sizes. (a) For motoneurone pool driving a larger muscle. (b) For a secondary muscle 50% smaller than (a). Shows the MVC when the current is maintained at the level that elicits the largest MVC values. The current levels were found experimentally.

For experimentally recorded isometric contractions, the contraction force produced is typically $< 25\%$ of the MVC [8] [18] [23] and the target value aimed for in experimentation with

the simulator is approximately 10% MVC.

4.2 Example simulation outputs

To demonstrate the utility of the simulation, the impact of shared branch inputs on coherence in motoneuorone pools is modelled. In the first model there are shared inputs from the motor cortex to the motoneurones driving two muscles. In the second model, these shared inputs are replaced by one-to-one mappings from the cortex of a motoneurone. Both sets of results were generated using 460 cortical neurones (400 excitatory, 60 inhibitory) with a 30% level of connectivity, 100 motoneurones and 10 interneurones and an overall delay of $\approxeq 20ms$ from the cortical input to muscle contraction. The rest of the simulation parameters are presented in Appendix C.3 in the form of a parameter file. The only significant change between the two models is that connectivity between the cortex and pool is reduced to one-to-one mappings from 30% connectivity.

4.2.1 Shared last order input

An example of the simulator's output is shown for two muscles (one 50% smaller than the other) being driven by the cortical sheet, where there is significant shared branching of the common drive into both motoneurone populations. Figures 4.2-4.8 show the data produced for two seconds of simulation time for illustration.

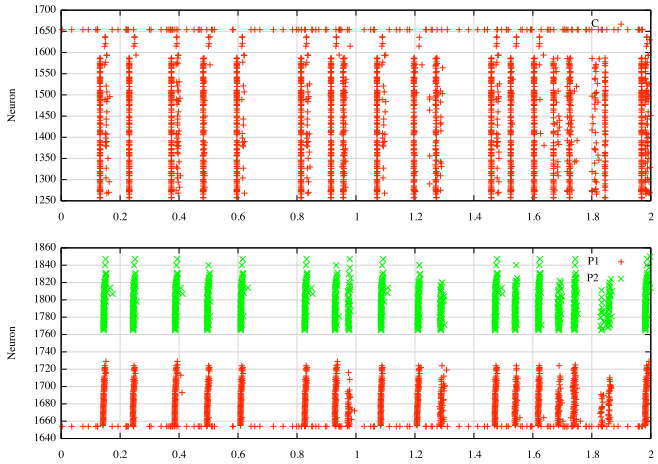

Figure 4.2: Spiking activity in the cortical sheet and motoneurone pools. (Top) Cortical sheet. (Bottom) The two motoneurone pools.

Figure 4.2 shows a time plot of spiking events in the core and motoneurone pools. The input signal to the sheet is shown in the top and bottom of the plots and has been set at 60Hz.

The cortical neurones show behaviour seen in pyramidal tract neurones where cycles of input are skipped, structuring their output into a more regular firing patterns.

Figures 4.3 shows a time plot of the membrane potentials for the point process input and a randomly selected sheet excitatory neurone, motoneurone and interneurone. Voltage adaptation effects can be clearly seen in the motoneurone's membrane trace. Figure 4.4 shows a time plot of a synaptic channels' PSP currents for randomly selected connections between the point process input and a sheet neurone, from a sheet neurone to a motoneurone and from the muscle to Golgi tendon and spindle organs.

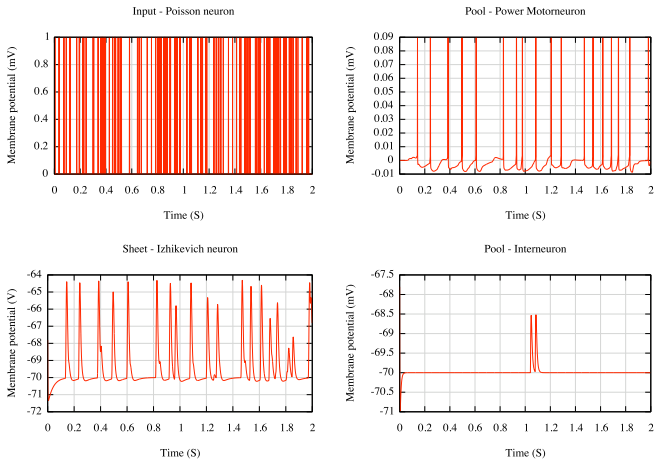

Figure 4.3: Membrane potential for simulated neurones. (TL) Point process neurone. (BL) Sheet neurone. (TR) Motoneurone. (BR) Interneurone.

Figure 4.5 shows the summed output for the simulated muscles during this time. Sustained contractions are not observed, as the activity of the motoneurone pools are poorly organised spatially and temporally. The GTO's response is ragged because the summed force falls repeatedly below its firing threshold.

The spike timing information of the motoneurones is then loaded into Matlab to provide EMG signals. The total number of fibres in muscle 1 is set at 130,000 and in muscle 2 at 90,000, compared to 45,000 for the first dorsal interosseus [56]. Figure 4.6 shows the simulated EMGs, recorded by two electrodes separated 5mm apart, for both muscles. The EMG signals further reflect the temporal separation of network activity.

The extracted EMG signals are then subjected first to Fourier Analysis via FFT and then further frequency and time analysis using the Neurospec package [26] (See Figures 4.7-4.8). FFTs of the the signals reveals no dominant frequencies but groupings around 2Hz and 25Hz frequencies in the cortical sheet. In the motoneurone pool result, there there is little clear grouping, with frequencies below 25Hz dominating the spectrum. Both pEEG-EMG signals show similar results in the Neurospec library, with the power-spectrum of the signals follow

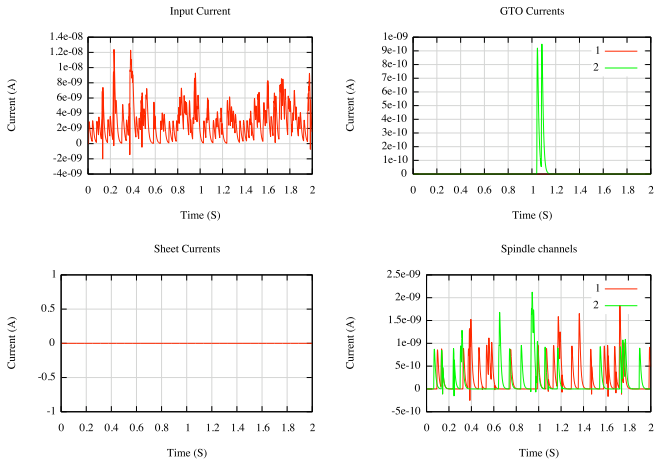

Figure 4.4: Invoked currents in synaptic channels. (TL) From the input to an excitatory neurone in the sheet. (BL) From a neurone in the sheet to a motoneurone. (TR) From GTOs to an inhibitory interneurone in the spinal code. (BR) From muscle spindles to motoneurones in the spinal code.

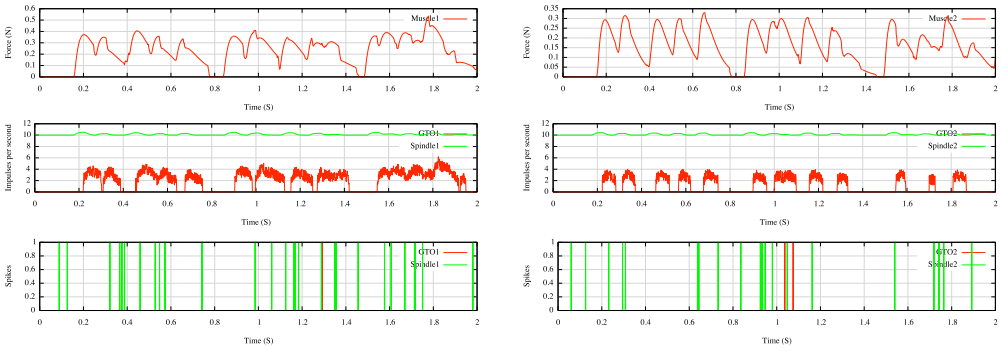

(a) Muscle1 and its afferents

(b) Muscle2 and its afferents

Figure 4.5: Muscle, GTO and spindle responses

similar time courses. The coherence estimates shows a strong relationship between the data at frequencies below 250Hz (the 95% confidence limit is shown by the dashed line) and the cumulant estimates show that the relationship is continuous throughout the time series (the solid black lines represent the upper and lower 95 % confidence levels) and is strongly centred around 20-30ms (the simulated projection time from cortex to muscle). EMG-EMG analysis shows a much strong coherence across all frequencies and a very strong time relationship centred around 0ms.

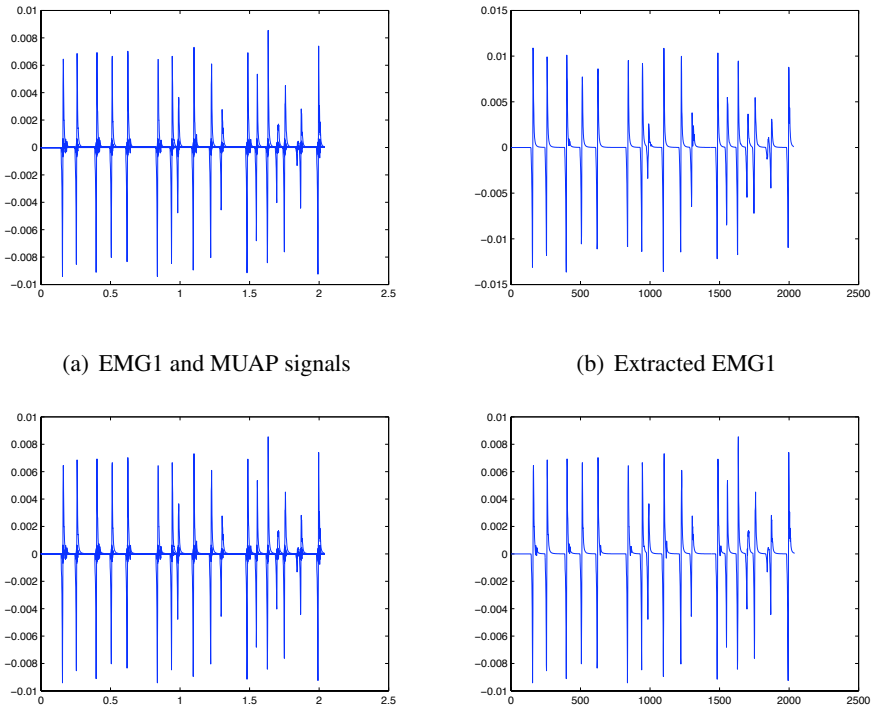

(a) EMG1 and MUAP signals

(b) Extracted EMG1

(c) EMG2 and MUAP signals

(d) Extracted EMG2

Figure 4.6: Extracted EMG signals. (TL) shows the MUAPs and EMG signal for the larger muscle. (TR) The EMG signal on its own. (BL) The MUAPs and EMG for the smaller muscle. (BR) The EMG on its own.

4.2.2 Isolating synchronicity in the motoneurone inputs

The common branch inputs are removed from the motor-pool and are replaced by one-to-one projections from the motor cortex to the motoneurones. The simulation is then run as before.

Figure 4.9 shows a time plot of spiking events in the core and motoneurone pools. In this simulation the cortical neurones show bursting behaviour but because the motoneurones receive only brief bursts of spikes from a single neurone, not all of them fire due their variable thresholds. The membrane potential and current plots show this clearly (See Figure 4.10). The

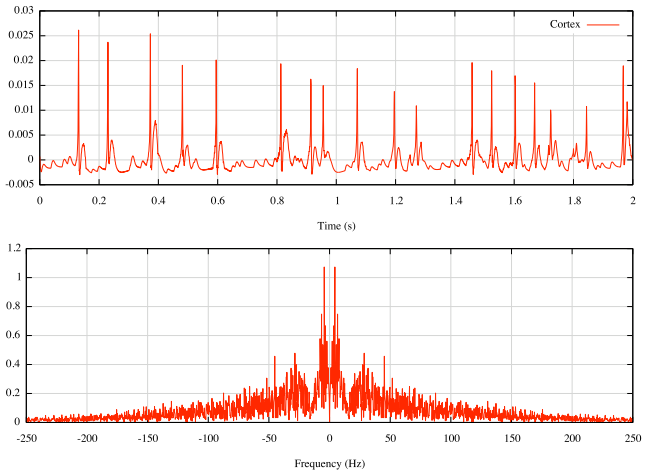

(a) FFT of Cortex LFP

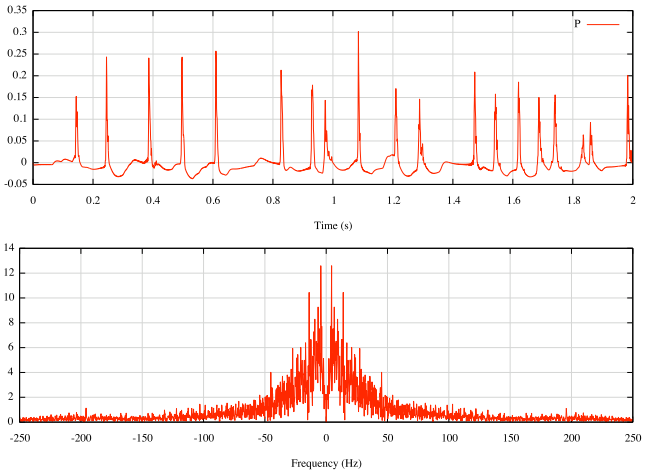

(b) FFT of Pool LFP

Figure 4.7: Fourier analysis of time series signals. (Top) pEEG. (Bottom) The summed activation potentials in the first motoneurone pool (Bottom).

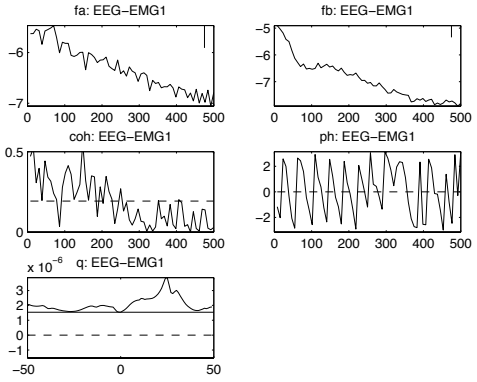

(a) EEG - EMG1

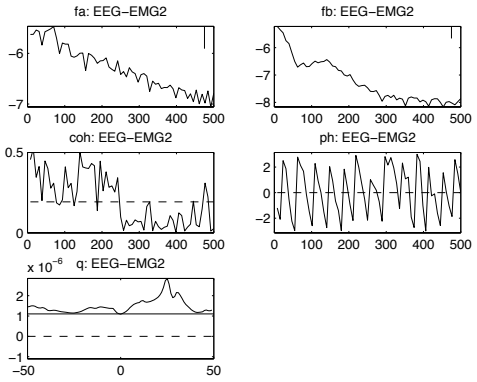

(b) EEG-EMG2

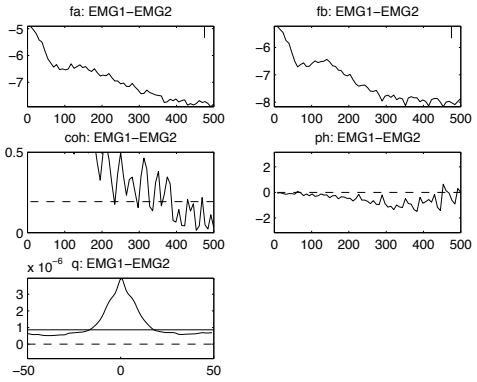

(c) EMG1-EMG2

Figure 4.8: Neurospec analysis of pEEG-EMG1 (Top), pEEG-EMG2 (Middle) and EMG1-EMG2 (Bottom).

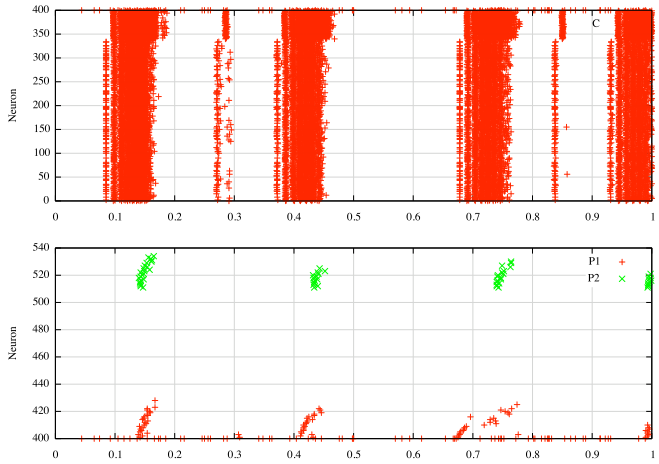

Figure 4.9: Spiking activity in the cortical sheet and motoneurone pools. (Top) Cortical sheet. (Bottom) The two motoneurone pools.

cortical neurone fires in bursts, but each PSP only slightly raises the membrane potential of the motoneurone and fewer PSPs arrive simultaneously than in Section 4.2.1. This reduced drive results in the motoneurone firing only once per concentrated burst. As there are few motoneurones firing concurrently, the muscle output is weak and discontinuous (Figure 4.12). This is illustrated by looking at the activity of the GTOs; the muscles' force is never strong enough to cause the GTO to respond.

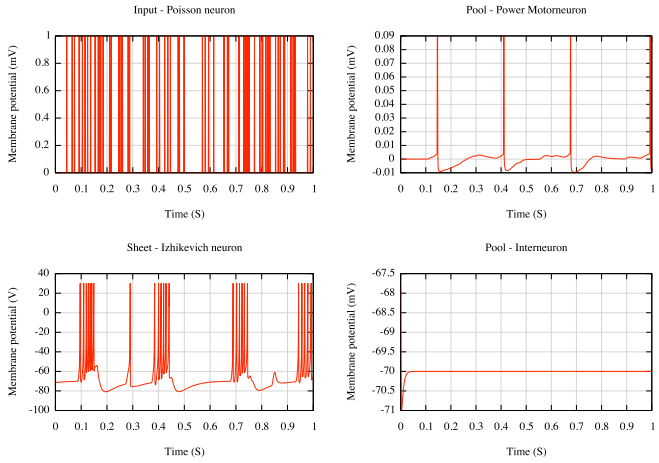

Figure 4.10: Membrane potential for simulated neurones

Figure 4.13 shows the simulated EMG recorded under the same settings as in the previous section. Time and frequency analysis is shown in Figures 4.14-4.15. The cortical bursting behaviour results in two clear groupings in the FFT results centred around 2Hz and 40Hz, while the weak response of the motoneurones results in no clear organisation in the LFP signal.

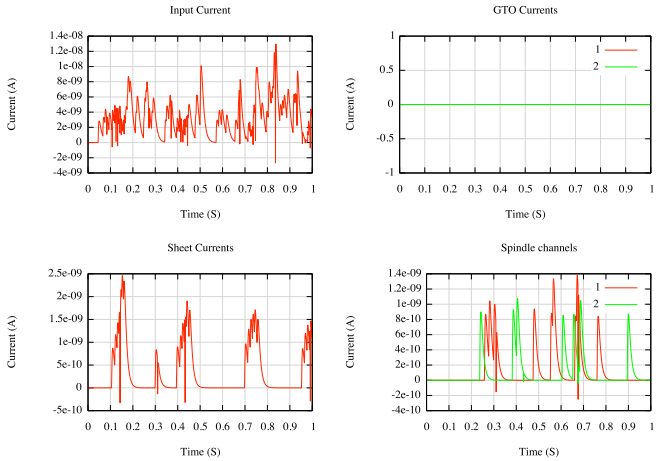

Figure 4.11: Invoked currents in synaptic channels. (Top) The summed muscle's twitch force. (Middle) The afferent's response in impulses per second. (Bottom) The spike trains of the afferent signals.

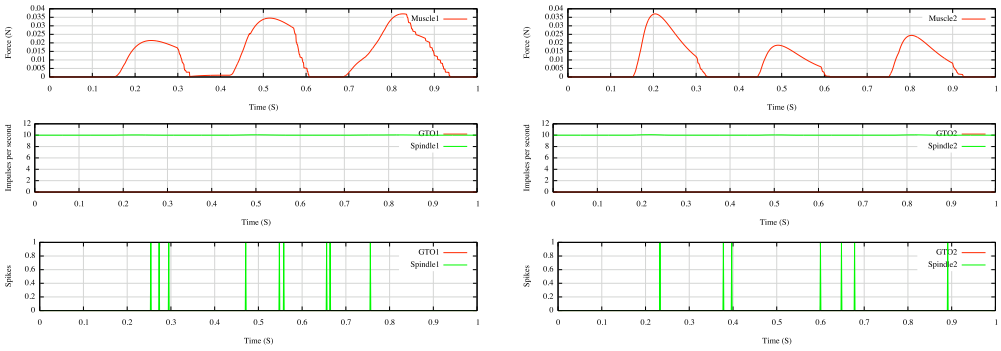

(a) Muscle1 and its afferents

(b) Muscle2 and its afferents

Figure 4.12: Muscle and spindle responses

Coherence between the signals is weaker than in Section 4.2.1 for all three time-series pairs, with coherence only seen below 20Hz and and in small higher frequencies for pEEG and EMG. EMG-EMG analysis shows that the signals have some small peaks of coherence and a flatter time relationship.

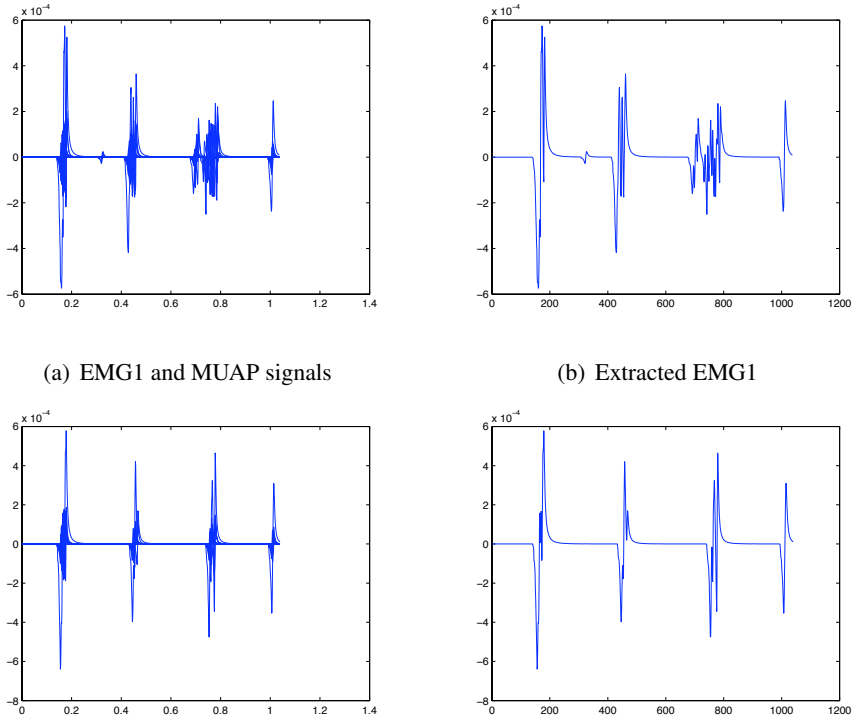

(a) EMG1 and MUAP signals

(b) Extracted EMG1

(c) EMG1and MUAP signals

(d) Extracted EMG2

Figure 4.13: Extracted EMG signals. (TL) shows the MUAPs and EMG signal for the larger muscle. (TR) The EMG signal on its own. (BL) The MUAPs and EMG for the smaller muscle. (BR) The EMG on its own.

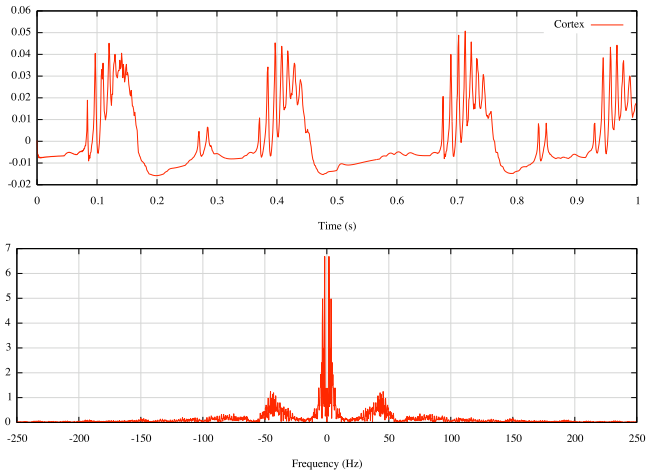

(a) EEG-LFP Coherence

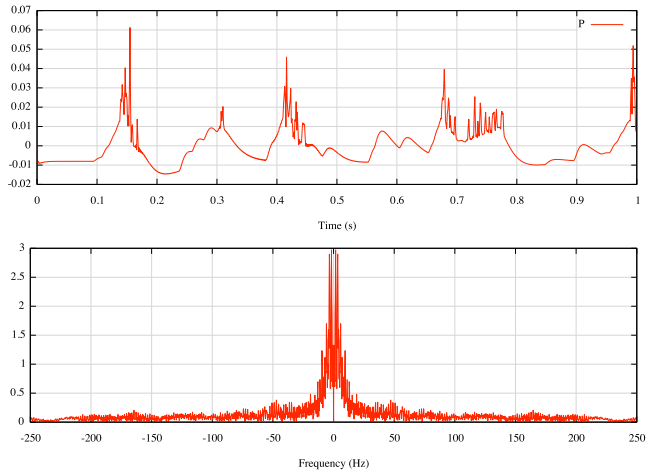

(b) EEG-EMG Coherence

Figure 4.14: Fourier analysis of time series signals. (Top) pEEG. (Bottom) Summed activation for the first motoneurone pool.

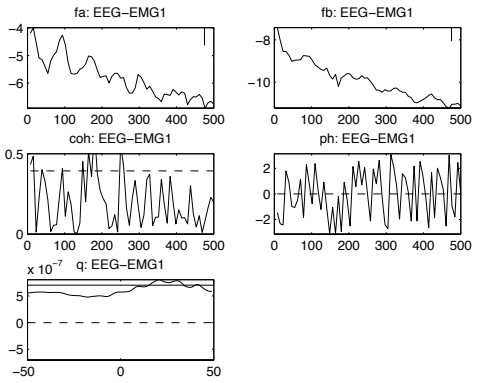

(a) pEEG-EMG1

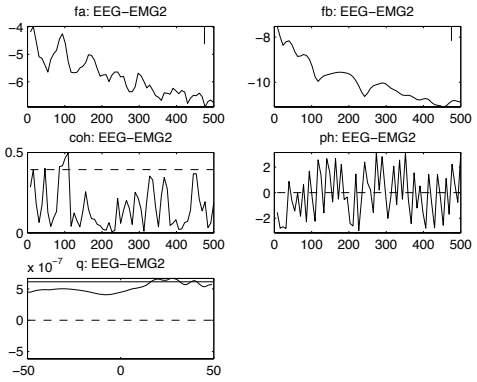

(b) pEEG-EMG2

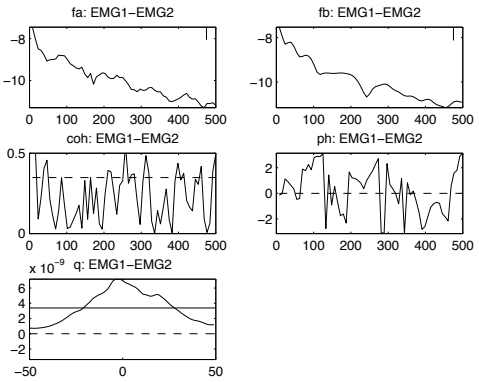

(c) EMG-EMG

Figure 4.15: Neurospec analysis of time series. (Top) pEEG-EMG1. (Middle) pEEG-EMG2. (Bottom) EMG-EMG.

Chapter 5

Conclusions and Future Work

5.1 Conclusion

The projection simulator described in this thesis provides an important research tool for exploring the developmental changes in common drive to motor-units. It provides a rich, complete model of the corticospinal tract including effectors and afferent feedback absent in previous simulation studies. The simulation also provides a mechanism for direct EEG-EMG and EMG-EMG time and frequency analysis allowing comparison with experimental research in human development of motor control.

Unfortunately, time constraints prevented the application of the simulation to investigate thoroughly developmental changes that could explain the changes in common drive reported by Farmer et al. [18]. Nevertheless, early results have provided tantalising glimpses of the potential usefulness of the simulation model to explore and generate new hypotheses that could drive future experimentation. The flexibility of the simulator suggest that it can not only be used to generate new hypothesis regarding the mechanisms responsible for the changes in motor-unit coherence observed, but also to gain understanding into the functional significance of such coherence.

Such oscillations may just be an occurrence of pure motor function forced by motor-unit preferred firing rates and the bio-physical properties of the muscles they innverate. Alternatively Baker et al. [3] theorise that oscillatory common drive maybe more efficient at recruiting motoneurones because the information carried in a oscillating synchronous signal is lower than that in an asynchronous signal. Consequently, the information processing requirements for isometric contractions are low enough to permit concomitant increases in synaptic efficacy that an oscillating descending command gives.

Another alternative is that oscillations occur around 20Hz because networks employing Beta rhythms are more effective at co-ordination over longer conduction delays than networks utilising Gamma rhythms. This increase in efficiency is due to the biophysical properties of the

long decay time of the slow currents [35] [44]. This fits in well with a self-organising view of corticospinal projections, where the oscillations are emergent.

It is hoped, that the Projection simulator presented in this thesis will prove to be a useful tool in explaining the developmental changes in muscle synchrony.

5.2 Limitations and extensions to the projection model

Due to the brief period of development there are many areas of the Projection simulator that require further thought to enhance the usefulness of the model.

Limitations

The major flaw in the current simulation model is that connections, while directed, are still formed at random during initialisation of the system. This randomisation prevents direct run-to-run comparison, as well as repeatability of results. The model requires a system to load and save network graphs that enable configurations to be tested repeatedly. Network assignment schemes [45] [32] should also be explored to provide biologically plausible cortical arrangements.

The secondary flaw is that there are a considerable number of parameters in the system which, while supporting very flexible simulation models, require considerable thought when setting up simulations especially because many of these parameters have dependencies on each other. Default parameter settings should be supplied as named groups to speed simulation construction.

While the model is comprised of sub-components created from previously published models, the connections between them are often based on approximations of the underlying biological systems. Where possible, guidance was used from previous modelling or experimental studies but it was not always known what the structure of these connections or their parameters should be. In particular, the connection between afferents and the cortex forming a secondary delay loop is poorly implemented and little information is received via this pathway during simulations. Further components may be required to aid the integration of afferent signals at this level, based on careful research.

Considering the simulator implements multiple sub-component models with rich dynamics and supports variable time-steps, the overall performance of the system is surprisingly good. Runs with nearly a 1000 neurones and 50,000 synaptic connections averaged 10s for each 1s of simulated time on a standard desktop PC. Nevertheless, there is a distinct trade-off in the complexity of the model (in terms of neurones and connections) versus the time for simulation. Execution time in the model is directly proportional to the number of synaptic connections created and the average level of spiking activity concurrent in the model. While the simulated

neurone models seem computationally efficient, it is the synaptic connections that seem to hinder performance. For certain experiments where exact PSP current dynamics are not required, the cortical sheet component could be replaced with a pulse-coupled network [32] enabling larger numbers of cortical neurones to be executed.

Extensions and future work

The most apparent missing component in the system is the ability to produce average firing information during simulation. Such information would be an indicator not only of the overall level of activity in the system but also an important part of matching experimental data. In an interesting development, Gibbs et al. [23] recorded that the average firing rate of thumb motor-units dropped from 16Hz before puberty to 13Hz in adults. Hockensmith et al. [29] reported that average firing rates of digit motor units in a contraction task was 9.8 ± 1.3 Hz. Currently, there is no straight-forward method to track firing rate information in the simulator.

One key aim of the project was to integrate afferent information because it is thought to play an important part in structuring coherence [52]. In previous models proprioceptive feedback has been all but ignored [3][42] [43] [56]. Only one study reviewed had any form of feedback from the muscles to the motoneurone pool [38] and this was in the form of an approximated error signal. While the model provides afferent responses, the signals modelled are basic and provide limited dynamics. The response of the afferents during the ramp phase of a contraction may be an important element that helps smooth motoneurone firing as well as having a potential impact on common drive. A secondary component, the γ motoneurone control system, was also ignored. The γ motoneurones play a significant part in controlling the responsiveness of the muscle spindles' singals [49] and further work is needed to measure their role, if any, in the changes in coherence observed.

Connectivity and neurone numbers can be changed to simulate pruning in simulators. However, no other plasticity mechanisms are currently modelled and some have theorised that the coherence phenomena observed has something to do with plasticity [23]. Spike-timing dependent plasticity (STDP) [55] was not considered in this study as its time frame (typically 1hr) is much smaller than the developmental time period being considered. However, if synaptic pruning is taking place, then STDP will have some effect in restructuring the remaining pathways, potentially creating networks where oscillatory behaviour dominates. Izhikevich has shown how integrating STDP with spiking neurone networks produces highly interesting dynamics [32].

Finally, the production of EMG, time and frequency analysis results is currently manually post-processed. To enable large-scale repeated testing with such simulation models, it is essential that not-only is all the information produce automatically but that there are also methods of automatic results extraction. The Neurospec code should be modified to provide the location

and value of the coherence peaks, while Matlab should integrated with C/C++ code base using the MEX interfaces.

Appendix A

Background Material

A.1 Powers' motoneurones

Figure A.1 shows the steady state activation of conductances for the four ionic channels in Powers' model (using the parameters from Table A.1). Each graph is centred on V_h, the voltage for half-activation and the slope is defined by the s parameter.

The two calcium channels activate first causing the depolarization of the neurone, which results in the membrane potential rising and leading ultimately to the generation of an action potential. The potassium channels activates at higher membrane potentials leading to hyper-polarization of the neurone and their activation results in recovery back to the resting potential - after hyper-polarization (AHP). Potassium activation-voltage curves are based on voltage-clamp experiments [48].

Channel	**vH** (mS)	**s** (mV^{-1})
gKs	45	7.5
gKf	45	4
gCal	16.5	2.5
gCah	28	3.5

Table A.1: Example vH and S values.

The steady-state relationship between membrane current and membrane voltage is shown in Figure A.2. Three graphs are presented: leak current only (I_l), leak current and potassium currents ($I_{ks} + I_l$) and all the channels (I_{tot}). The curve for I_{tot} shows an 'n' shaped I-V curve, similar to that observed in cat motoneurones [48].

Zengel et al [57] recorded the electrical properties in cat α motoneurones for Slow (S), Fast twitch with intermediate fatigue resistance (FI), Fast twitch, fatigue-resistant (FR) and Fast twitch, fast fatiguing (FF) motor-units (MU); data for capacitance C and leakage current gL is

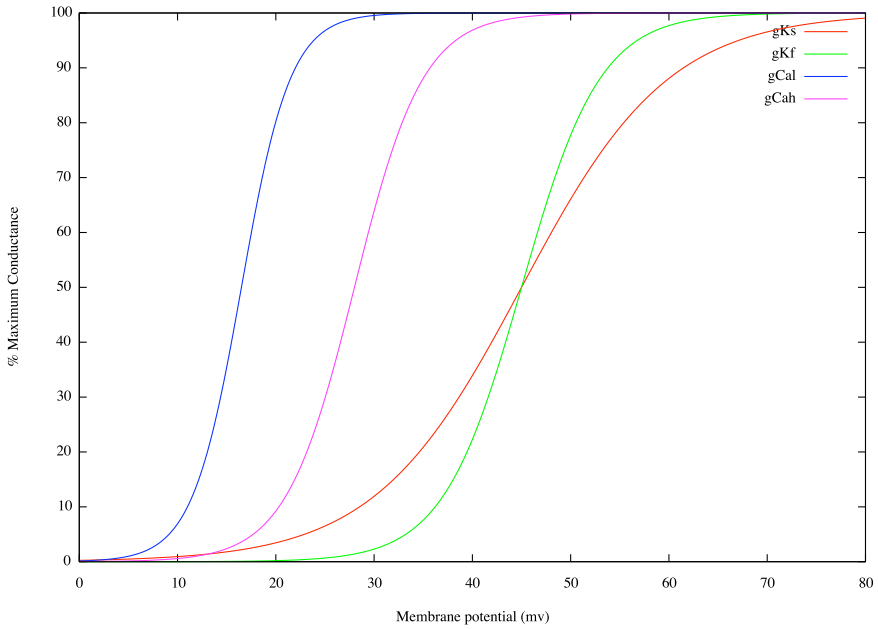

Figure A.1: Steady state activation values for the four ionic channels in Powers' motoneurone model. gKs is the slow potassium channel, gKf is the fast potassium channel, $gCal$ is the low-threshold calcium channel and $gCah$ is the high-threshold calcium channel.

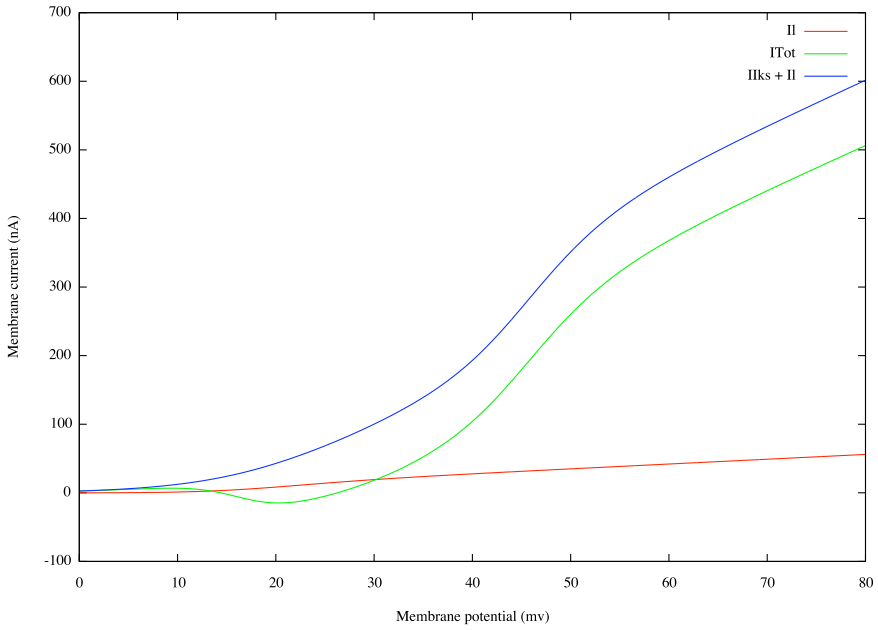

Figure A.2: Steady state membrane voltage and current relationships in Powers' motoneurones.

shown in Table A.2. This experimental data can be used to parameterise the model neurone allowing comparison against published data. While this data drawn from recorded values for cat α motoneurones, it demonstrates the flexibility of Powers' model.

It can be shown that Powers' motoneurones can approximate the AHP recovery curves found experimentally (See Figures A.3 and A.4). The graphs also demonstrate the impact of leakage conductance and capacitance on the AHP curves produced.

MU type	**gL** (*muS*)	**C** (*nF*)
S	0.63	6.5
FR	1.1	8.8
FI	1.42	7.5
FF	1.66	9.8

Table A.2: Reported mean capacitance and leakage current values for cat α motoneurones [57]

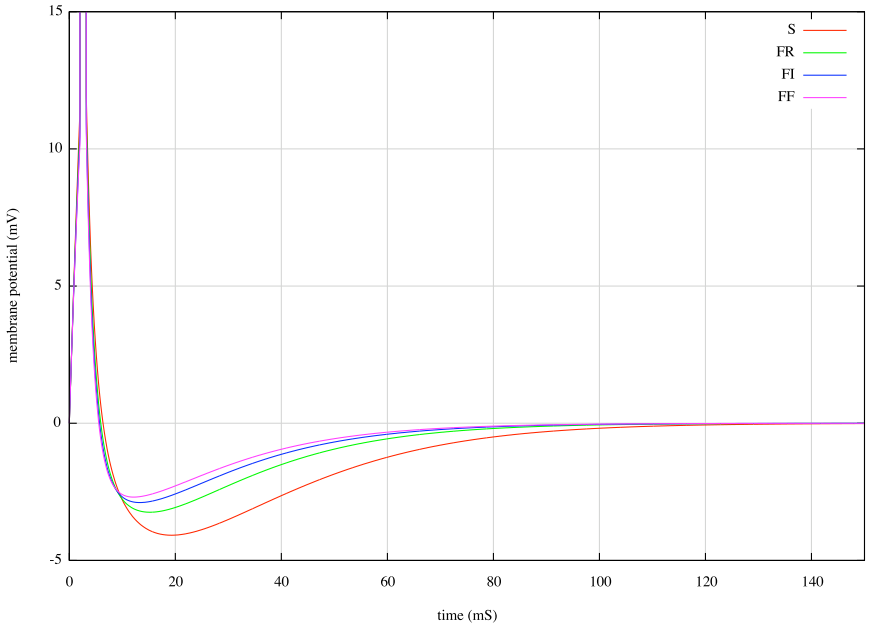

Figure A.3: Membrane potential of model motoneurone using a fixed capacitance $C = 8.1\ nF$ with varying values of gL. Leakage conductance is small for the slowest MU and rises for the faster MUs.

A.2 Synaptic channel model

The output of the channel is controlled by the onset (time after spike that the channel responds) and the delay (decay period for the response). The onset models the delay between an impulse

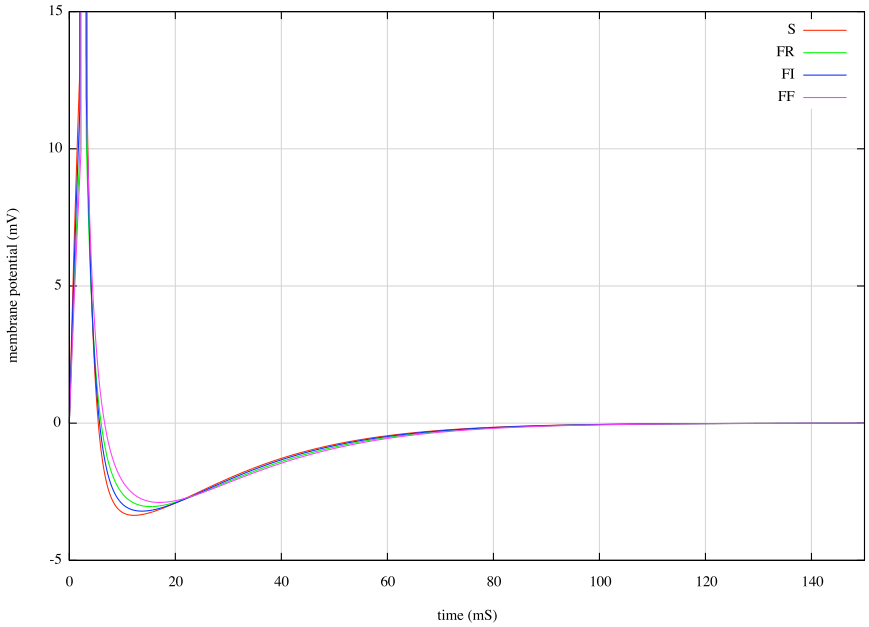

Figure A.4: Membrane potential of model motoneurone using a fixed leakage conductance $gL = 1.2\ \mu S$ with varying values of C. Neurone capacitance is small for the slowest MU and rises for the faster MUs.

arriving at the synapse and the triggering of a PSP. Figure A.5 shows the output of equation 3.7 for three spikes, each separated by 25 mS.

Figure A.6 shows how the time course of EPSP and IPSP with Kudela et als [36] model changes, with the membrane potential of the post synaptic spike. The post-synaptic membrane voltage is held at rest (-72mV), at its spiking value (30mV) and at the lower limit of the hyper-polarization period (-100mV) for both an excitatory and inhibitory connection with: T_d = 10 mS, T_o=3 mS, $w = 1$. E_{syn} = -10mV for the excitatory connection and $-72mV$ for the inhibitory

Figure A.7 shows the time courses for the revised model, reflecting experimental data [22] (see Section 3.3 for further details of this modification).

A.3 Twitch model

Figure A.8 shows the force output of Motoneurones 1, 50 and 100 firing with a fixed inter-spike interval (ISI) of 10ms. The twitch model output at this frequency is 40%, 21% and 11% of the peak twitch force for motoneurones 1, 50, and 100 respectively. The percentage of force output is controlled by the gain function, which has a mostly sigmoid form based on the relationship of contraction time and interspike interval - see equations (3.18 - 3.22).

The figure shows the twitch force reaches its peak value in the given twitch contraction time.

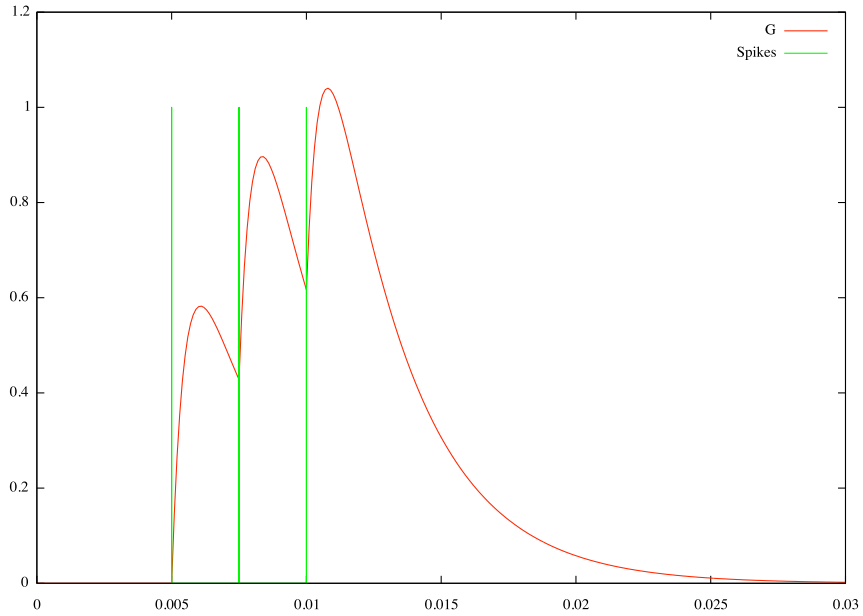

Figure A.5: Summation of spiking in synaptic connection model showing three spikes and the invoked PSP currents generated.

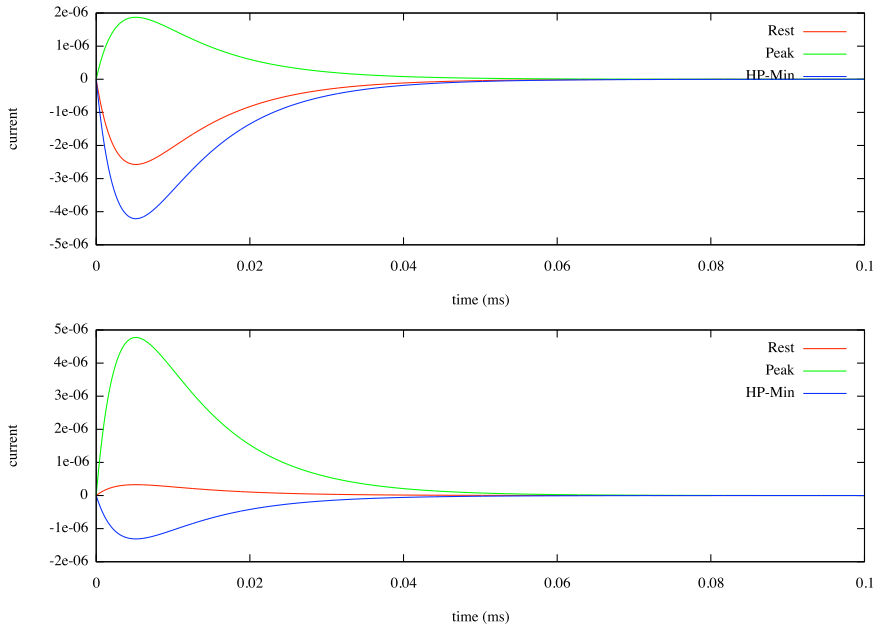

Figure A.6: Time course of post-synaptic potentials with varying membrane potentials. (Top) Excitatory connection. (Bottom) Inhibitory.

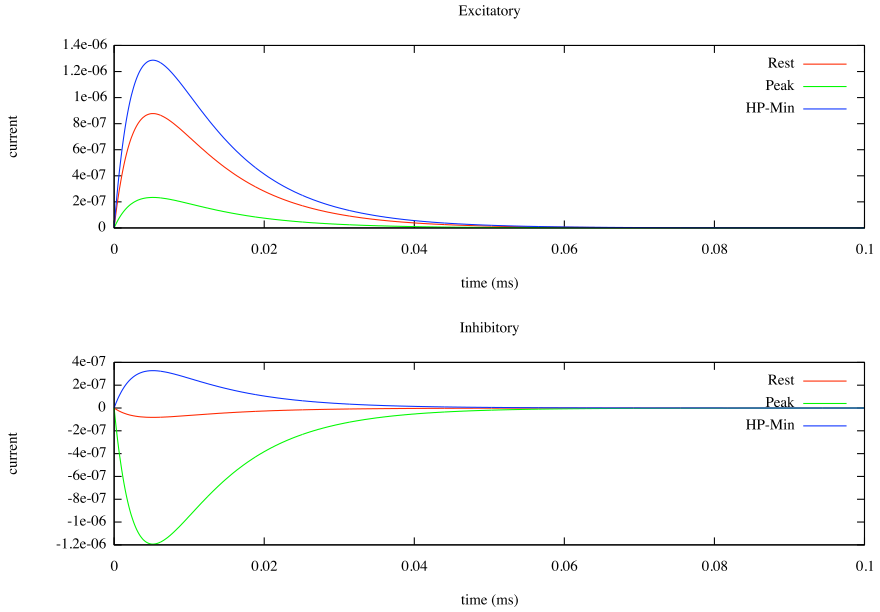

Figure A.7: Time course of post-synaptic potentials with varying membrane potentials with modified channel function. (Top) Excitatory connection. (Bottom) Inhibitory.

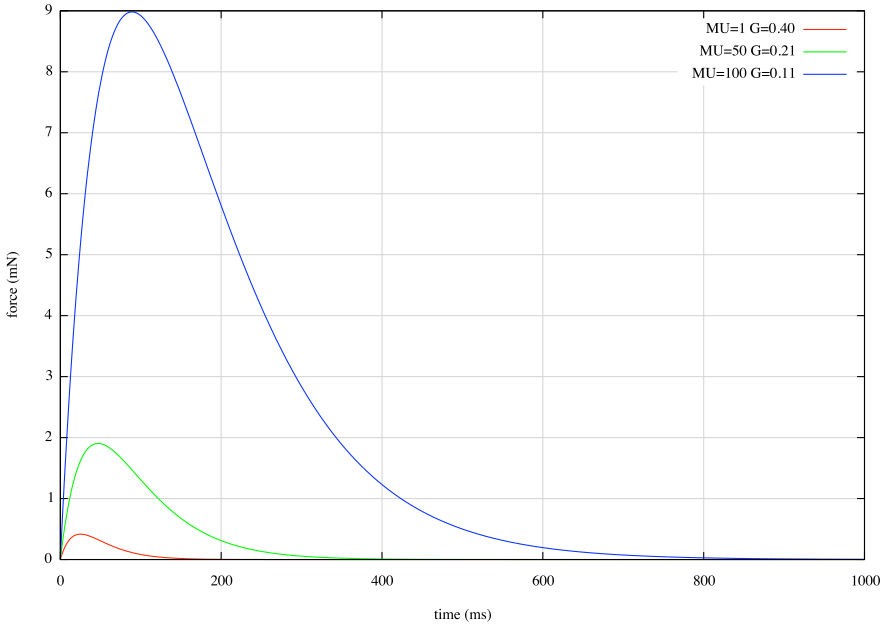

Figure A.8: Simulated twitch forces for neurones firing with a constant ISI of 10mS for three motor-units. Motor-unit 1 being the smallest and motor-unit 100 the largest.

A.4 EMG

Simulated EMG is generated using the dipole model of Fuglevand et al [21]. There is a subtle problem in this simple model, which leads to a instantaneous voltage potential at time zero during simulation of potential. This offset occurs because the model assumes that the source and sink currents appear instantaneously in the end plate zone when an action potential arrives from the driving motoneurone. This effect can be seen in Figure A.9.a, where the starting potential in the model is non-zero resulting in a step to appear to in simulation.

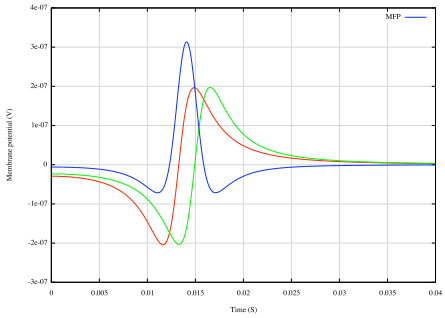

(a) Fibre potential recorded without current adaptation. Electrode distance=5mm

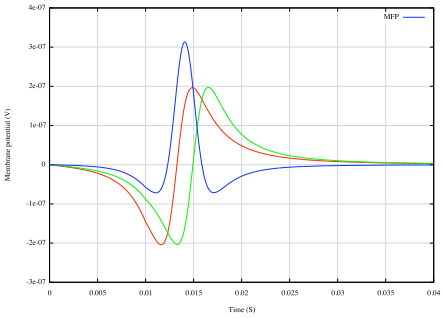

(b) Fibre potential recorded with current adaptation. Electrode distance=5mm

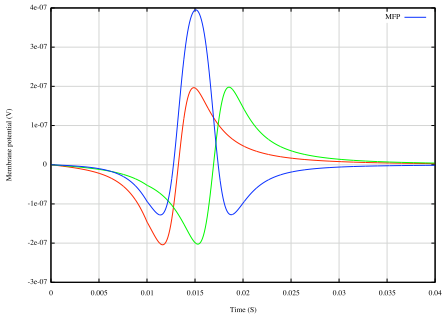

(c) Fibre potential recorded with current adaptation. Electrode distance=11mm

Figure A.9: **Simulation of muscle fibre potentials**. (a) Shows recorded potentials for two point electrodes on a typical muscle fibre (t = 0, is the time of the generation of the potential in the muscle's end plate). The potential recorded between them shows a triphasic muscle fibre potential. Without current adaptation there is an instantaneous offset at t = 0 in (a). In (b) with adaptation the potential changes smoothly in a more biologically plausible fashion. (c) Shows the change in MFP when the electrodes are 11mm apart.

These step effects are removed by modifying the current model so that source and sink currents linearly grow from zero to the dipole current value ($\pm 388\eta$A in the models), reflecting a more physiologically realistic model [19]. Figure A.9.b shows how the current adaptation to Fuglevand's model results in the removal of the offset effect (Appendix B.4 contains the Matlab

code which produced this example).

Figure A.10 shows the recording made by a single electrode recording a single muscle fibre potential at differing depths. Figure A.11, shows a small section of simulated EMG. See [21] for details.

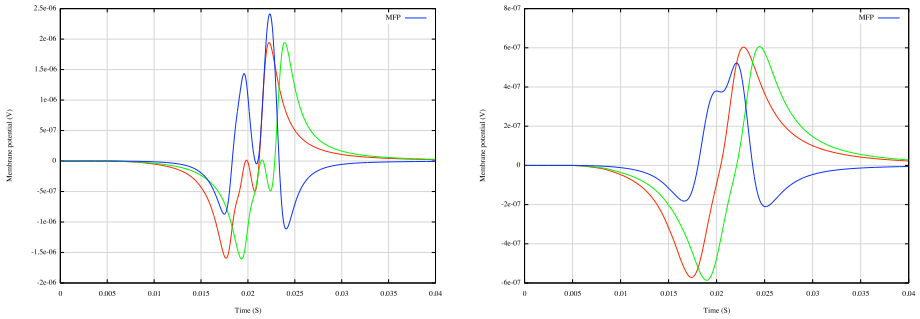

(a) Fibre potential recorded at 1.5mm (b) Fibre potential recorded at 3.0mm

Figure A.10: **Simulation of muscle fibre potentials at different depths**. (a) Shows two electrode recordings at a depth of 1.5mm with a motoneurone spiking at 5ms, 6.2ms, 8ms and 8.4ms. The effects of individual motor-unit action potentials are visible in the muscle fibre's potential (b) Same simulation but electrodes were 3mm away from muscle fibre. The signal is much smoother and has suffered nearly an order of magnitude loss in amplitude.

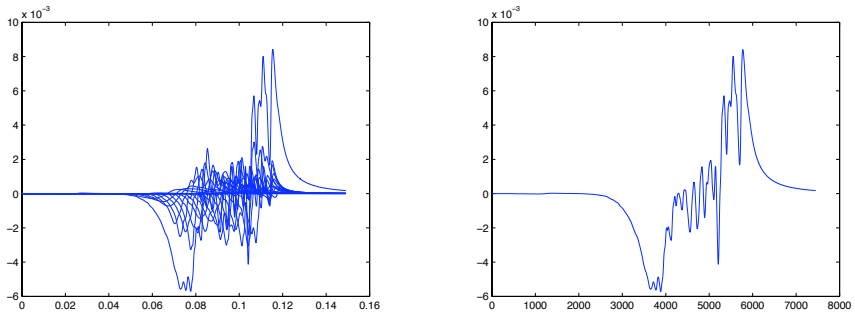

(a) Calculated MUAPs and EMG (b) Extracted EMG signal

Figure A.11: **Simulated EMG signal** (a) shows individual MUAPs for a muscle with 20 motor-units responding to a concentrated burst of spikes. (b) shows the extracted EMG.

Bibliography

[1] P. Ashby and D. Zilm. Relationship between epsp shape and cross-correlation profile explored by computer simulation for studies on human motoneurons. *Experimental Brain Research*, 47(1):33–40, 1982.

[2] S. Baker. Quantification of the relative efficacies of asynchronus and oscillating inputs to a motoneurone pool using a computer model. *Journal of Physiology*, 504(P):116, 1997.

[3] S. Baker, J. Kilner, E. Pinches, and R. Lemon. The role of synchrony and oscillations in the motor output. *Experimental Brain Research*, 128:109–117, 1999.

[4] S. Baker and R. Lemon. A computer simulation for investigation of the contribution of presynaptic synchrony to post spike facilitation in spike-triggered averages of rectified emg. *Journal of Physiology*, 483.P:28–29, 1995.

[5] S. Baker and R. Lemon. Computer simulation of post-spike facilitation in spike-triggered averages of rectified emg. *Journal of Neurophysiology*, 80(3):1391–1406, 1998.

[6] A. Brovelli, M. Ding, A. Ledberg, Y. Chen, R. Nakamura, and S. L. Bressler. Beta oscillations in a large-scale sensorimotor cortical network: Directional influences revealed by granger causality. *Proceedings of the National Academy of Sciences*, 101(26):9849–9854, 2004.

[7] W. Calvin and C. Stevens. Synaptic noise and other sources of randomness in motorneuron interspike intervals. *Journal of Neurophysiology*, 31:574–587, 1968.

[8] A. Carpentier, J. Duchateau, and K. Hainaut. Motor unit behaviour and contractile changes during fatigue in the human first dorsal interosseus. *Journal of Physiology*, 534(3):903–912, 2001.

[9] Y. Choe and R. Miikkulainen. The role of postsynaptic potential decay rate in neural synchrony. *Neurocomputing*, 52-54:707–712, 2003.

[10] A. R. Clarke, R. J. Barry, R. McCarthy, and M. Selikowitz. Age and sex effects in the eeg: development of the normal child. *Clinical Neurophysiology*, 112(5):806–814, 2001.

[11] C. Clopath, R. Jolivet, A. Rauch, H.-R. Lüscher, and W. Gerstner. Predicting neuronal activity with simple models of the threshold type: Adaptive exponetial integrate-and-fire models with two compartments. *Neurocomputing*, 70:1668–1673, 2006.

[12] B. Conway, D. Halliday, S. Farmer, U. Shahani, P. Mass, A. Weir, and J. Rosenburg. Synchronization between motor cortex and spinal motoneuronal pool during the performance of a maintained motor task in man. *Journal of Physiology*, 489(3):917–924, 1995.

[13] P. Crago, J. Houk, and W. Rymer. Sampling of total muscle force by tendon organs. *Journal of Neurophysiology*, 47(6):1069–1083, 1982.

[14] A. Datta, S. Farmer, and J. Stephens. Central nervous pathways under lying synchronization of human motor unit firing studied during voluntary contractions. *Journal of Physiology*, 432(1):401–425, 1991.

[15] P. Dayan and L. Abbot. *Theoretical Neuroscience: Computational and Mathematical Modeling of Neural Systems*. MIT Press, Decemeber 2005.

[16] B. B. Edin and A. B. Vallbo. Muscle afferent responses to isometric contractions and relaxations in humans. *Journal of Neurophysiology*, 63(6):1307–1313, 1990.

[17] S. Farmer. Personal communications. 2007.

[18] S. Farmer, J. Gibbs, D. Halliday, L. Harrison, L. James, M. Mayston, and J. Stephens. Changes in emg coherence between long and short thumb abductor muscles during human development. *Journal of Physiology*, 579(2):389–402, 2007.

[19] A. J. Fuglevand. Personal communications. August 2007.

[20] A. J. Fuglevand, D. A. Winter, and A. E. Patla. Models of recruitment and rate coding organization in motor-unit pools. *Journal of Neurophysiology*, 70(6):2470–2488, 1993.

[21] A. J. Fuglevand, D. A. Winter, A. E. Patla, and D. Stashuk. Detection of motor unit action potentials with surface electrodes: influence of electrode size and spacing. *Biological Cybernetics*, 67(2):143–153, 1992.

[22] W. Gerstner and W. Kistler. *Spiking Neuron Models*. Cambridge University Press, 2002.

[23] J. Gibbs, L. Harrison, and J. Stephens. Cross-correlation analysis of motor unit activity recorded from two separate thumb muscles during development in man. *Journal of Physiology*, 499:255–266, 1997.

[24] N. Gogtay, J. Gield, L. Lusk, K. Hayashi, D. Greenstein, A. Vaituzis, T. Nugent, D. Herman, L. Clasen, A. Toga, J. Rapoport, and P. Thompson. Dynamic mapping of human

cortical development during childhood through early adulthood. *Proceedings of the National Academy of Sciences*, 101(21):8174–8179, 2004.

[25] E. R. Gossen, T. D. Ivanova, and S. J. Garland. The time course of the motoneurone afterhyperpolarization is related to motor unit twitch speed in human skeletal muscle. *Journal of Physiology*, 552(2):657–664, 2003.

[26] D. Halliday. Neurospec, http://www.neurospec.org.

[27] D. Halliday, B. Conway, S. Farmer, and J. Rosenburg. Using electroencephalography to study functional coupling between cortical activity and electromyograms during voluntary contractions in humans using electroencephalography to study functional coupling between cortical activity and electromyograms during voluntary contractions in humans. *Neuroscience Letters*, 241:5–8, 1998.

[28] D. Halliday, J. Rosenburg, B. P. Amjad, A.M., B. Conway, and S. Farmer. A framework for the analysis of mixed time series/point process data - theory and application to the study of physiological tremor, single motor unit discharges and electromyograms. *Progress in Biophysics and Molecular Biology*, 64(2-3):237–78, 1995.

[29] G. Hockensmith, S. Lowell, and A. J. Fuglevand. Common input across motor nuclei mediating precision grip in humans. *Journal of Neuroscience*, 25(18):4560–4564, 2005.

[30] E. Izhikevich. Simple model of spiking neurons. *IEEE Transactions on Neural Networks*, 14(6):1569–1572, 2003.

[31] E. Izhikevich. Which model to use for cortical spiking neurons? *IEEE Transactions on Neural Networks*, 15:1063–1070, 2004.

[32] E. Izhikevich, J. Gally, and G. Edelman. Spike-timing dynamics of neuronal groups. *Cerebal Cortex*, 14:933–944, 2004.

[33] J. K. S. Jansen and P. B. C. Matthews. The central control of the dynamic response of muscle spindle receptors. *Journal of Physiology*, 161(2):357–378, 1962.

[34] P. Kirkwood and T. Sears. Cross-correlation analyses of motoneuron inputs in a coordinated motor act. In Kruger, editor, *Neuronal Cooperativity*, pages 225–248. Springer-Verlag, 1991.

[35] N. Kopell, G. Ermentrout, M. Whittington, and R. Traub. Gamma rhythms and beta rhythms have different synchronization properties. *Proceedings of the National Academy of Sciences*, 97:1867–1872, 2000.

[36] P. Kudela, P. Franaszczuk, and G. Bergey. A simple computer model of excitable synaptically connected neurons. *Biological Cybernetics*, 77:71–77, 1997.

[37] P. Kudlea, P. J. Franaszczuk, and G. K. Bergey. Changing excitation and inhibition in simulated neural networks: effects induced on bursting behavior. *Biological Cybernetics*, 88(4):276–285, 2002.

[38] M. M. Lowery and Z. Erim. A simulation study to examine the effect of common motoneuron inputs on correlated patterns of motor unit discharge. *Journal of Computational Neuroscience*, 19(2):107–124, 2005.

[39] M. D. Mann. *The Nervous System and Behavior: An Introduction*. Harper and Row, revised online as 'the nervous system in action' (http://www.unmc.edu/physiology/mann) edition, (Accessed June 2007) 1981.

[40] M. P. Mileusnic and G. E. Loeb. Mathematical models of proprioceptors. ii. structure and function of the golgi tendon organ. *Journal of Physiology*, 96(1789-1802), 2006.

[41] A. Monster and H. Chan. Isometric force production by motor units of extensor digitorum communis muscle in man. *Journal of Neuroscience*, 40(1432-1443), 1977.

[42] L. Myers, Z. Erim, and M. Lowery. Time and frequency domain methods for quantifying common modulations of motor unit firing patterns. *Journal of NeuroEngineering and Rehabilitation*, 1(2), 2004.

[43] R. Nussbaumer, D. Ruegg, L. Studer, and J.-P. Gabriel. Computer simulation of the motoneuron pool–muscle complex. i. input system and motoneuron pool. *Biological Cybernetics*, 86(4):317–333, 2002.

[44] M. Olufsen, M. Whittington, M. Camperi, and N. Kopell. New roles for the gamma rhythm: Population tuning and preprocessing for the beta rhythm. *Journal of Computational Neuroscience*, 14:33–54, 2003.

[45] Q. Pauluis, S. Baker, and E. Oliver. Emergent oscillations in a realistic network: The role of inhibition and the effect of the spatiotemporal distribution of the input. *Journal of Computational Neuroscience*, 6:27–48, 1999.

[46] T. Paus. Mapping brain maturation and cognitive development during adolescence. *Trends in Cognitive Science*, 9(2):60–68, 2005.

[47] R. Powers. A variable-threshold motoneuron model that incorporates time- and voltage-dependent potassium and calcium conductances. *Journal of Neurophysiology*, 70(1):246–262, 1993.

[48] R. Powers and M. Binder. Effective synaptic current and motoneuron firing rate modulation. *Journal of Neurophysiology*, 74(2):793–801, 1995.

[49] A. Prochazka and G. Gorassini. Models of ensemble firing of muscle spindle afferents recorded during normal locomotion in cats. *Journal of Physiology*, 507(1):277–291, 1998.

[50] D. Purves, G. J. Augustine, D. Fitzpatrick, W. Hall, A. LaMantia, J. McNamara, and S. Williams. *Neuroscience*. Sinauer Associates Inc, 3rd edition, 2004.

[51] A. Rauch, G. L. Camera, H.-R. Lüscher, W. Senn, and S. Fusi. Neocortical pyramidal cells respond as integrate-and-fire neurons to in vivo–like input currents. *Journal of Physiology*, 90:1598–1612, 2003.

[52] C. Riddle and S. Baker. Manipulation of peripheral neural feedback loops alters human corticomuscular coherence. *Journal of Physiology*, 566(2):625–639, 1995.

[53] M. Santello and A. J. Fuglevand. Role of across-muscle motor unit synchrony for the coordination of forces. *Experimental Brain Research*, 159:501–508, 2004.

[54] M. Schieber and A. J. Fuglevand. Motor areas of the cerebal cortex. In *Encyclopedia of Cognitive Science*, pages 111–121. Nature Publishing Group, 2003.

[55] S. Song, K. D. Miller, and L. Abbot. Competitive hebbian learning through spike-timing dependent synaptic plasticity. *Nature Neuroscience*, 3(9):919–929, 2000.

[56] W. Yao, A. J. Fuglevand, and R. M. Enoka. Motor-unit synchronization increases emg amplitude and decreases force steadiness of simulated contractions. *Journal of Neurophysiology*, 83(1):441–452, 2000.

[57] J. Zengel, S. Reid, G. Sybert, and J. Munson. Membrane electrical properties and prediction of motor-unit type of medial gastrocnemius motoneurons in the cat. *Journal of Neurophysiology*, 53(5):1323–1344, 1985.